Initiation of neutralizing antibody response probed using synthetic virus-like structures

Wei-Yun Wholey[1†], Alexander R. Meyer[1†], Sekou-Tidiane Yoda[1], Bryce Chackerian[2], Julie Zikherman[3], Wei Cheng[1,4]*

[1]*Department of Pharmaceutical Sciences, 428 Church Street, University of Michigan, Ann Arbor, Michigan 48109, USA*

[2]*Department of Molecular Genetics and Microbiology, School of Medicine, University of New Mexico, Albuquerque, New Mexico 87131, USA*

[3]*Division of Rheumatology, Rosalind Russell and Ephraim P. Engleman Arthritis Research Center, Department of Medicine, University of California, San Francisco, California 94143 USA*

[4]*Department of Biological Chemistry, 1150 W. Medical Center Dr., University of Michigan Medical School, Ann Arbor, Michigan 48109, USA*

†: Both authors contributed equally to this work.

Classifications: biological sciences, microbiology

Keywords: virus-like structures, epitope density, nucleic acids, antibody

*Corresponding author:

Dr Wei Cheng
University of Michigan
428 Church Street
Ann Arbor, MI, 48109-1065
Tel: (734) 763-3709
Fax: (734) 615-6162

E-mail address: chengwe@umich.edu

Abstract

Class-switched neutralizing antibody (nAb) production is rapidly induced upon many viral infections. However, due to the presence of multiple components in virions, the precise biochemical and biophysical signals from viral infections that initiate nAb responses are unknown. Using a reductionist system of synthetic virus-like structures (SVLS) containing minimal, highly purified biochemical components commonly found in enveloped viruses (1, 2), here we show that a foreign protein on a virion-sized liposome can serve as a stand-alone danger signal to initiate class-switched nAb response in the absence of cognate T cell help or Toll-like receptor signalling. These liposomal structures become highly potent inducers of nAb with internal DNA or RNA. As early as day 5 after injection, as low as a few molecules of surface antigen and as little as 100 ng of antigen can induce all IgG subclasses known in mice and potent nAb production. The IgG titers rival those induced by bacteriophage virus-like particles at the same antigen dose. Potent induction of IgG can even occur in mice deficient in CD19, a B cell coreceptor important for vaccine efficacy in humans. Our results rationalize the immunogenicity of virus-like particles and demonstrate a generalized mechanism for nAb induction upon viral infection in mice, with the minimal structures of viruses alone being potent inducers of nAb, without viral replication or any other components. The SVLS system will be useful for broader understanding of viral immunogenicity in mammals, which may enable highly efficient activation of antigen-specific B cells for prophylactic or therapeutic applications.

Significance statement

Neutralizing antibody is rapidly induced upon many viral infections, but the underlying mechanisms remain incompletely understood. Here we show that several features of this antibody response can be reconstituted by synthetic virus-like structures containing minimal, highly purified biochemical ingredients commonly found in enveloped viruses, and without any other components. These findings reveal a shared mechanism to produce neutralizing antibodies upon viral infection. A few molecules of surface antigen on a virion-sized sphere, when combined with nucleic acids within these structures, can trigger strong antiviral IgG production. These findings have broad implications on mechanisms of neutralizing antibody induction, including that of SARS-CoV-2. The minimum system discovered here will be useful for prophylactic or therapeutic applications.

Main text

Studies of humoral immunity upon viral infection have revealed many common features of antibody responses towards both icosahedral and enveloped viruses (3-7). For the majority of viruses, these antibodies are induced rapidly, within just a few days after infection (6). These early antibodies are isotype class-switched independent of $CD4^+$ T cells (5, 8-10), and are potent in viral neutralization (5, 8-10). In some cases, the antibody production can last very long after the resolution of primary infections (7, 11). These common features suggest shared mechanisms in B cell sensing and response to viral particulate antigens (Ags). Studies using inactivated viruses (3, 12) have established the significance of high repetitiveness of viral antigens for the induction of neutralizing antibodies (nAbs). However, due to the presence of multiple viral components in these particles, the precise biochemical and biophysical signals from viral infections that initiate a nAb response remain unknown.

The characterization and the use of synthetic virus-like structures

To identify the minimal but common features in enveloped viruses that trigger nAb response upon viral infection, we have developed a reductionist system of synthetic virus-like structures (SVLS). We constructed SVLS using highly purified biochemical components found in enveloped viruses and engineered them to resemble the common biophysical features of naturally occurring enveloped viruses (1, 2, 13). Existing platforms such as virus-like particles (VLPs) (14, 15), ferritin nanoparticles (16) or computationally designed self-assembling protein nanomaterials (17) have been extensively studied and used in vaccine design and development. However, they all use immunogenic foreign proteins as their structural scaffolds for antigen display. To unravel the molecular basis of virion

immunogenicity, the SVLS system herein uses lipid bilayers (18) instead of foreign proteins to serve as the scaffold of SVLS, eliminating immune responses towards the scaffolds themselves, which may complicate data interpretation. In fact, we selectively chose lipids that were abundant in natural plasma membranes to construct SVLS (Materials and methods). To mimic naturally occurring viruses, we also avoided cationic lipids that are known to be immunostimulatory in nature (19), which were extensively used especially recently for the therapeutic delivery of nucleic acids (20). In addition, this system allows us to encapsulate purified nucleic acids with *all-natural* phosphodiester backbone inside SVLS, which mimics the spatial confinement and chemical composition of a typical viral genome (1, 2). The role of internal nucleic acids (iNA) on nAb responses has not been investigated using either ferritin or computationally designed self-assembling protein nanomaterials.

We have prepared four sets of SVLS for current study: two of them, schematically shown in Fig. 1A and B insets and termed pRBD and pHEL, respectively, are SVLS that display either purified receptor-binding domain (RBD) of the SARS-CoV-2, the causative agent of the COVID-19 pandemic (21); or a purified hen egg lysozyme (HEL) mutant, a well-established model antigen for immunology studies. These two proteins are completely unrelated in both structures and evolution. Each protein was displayed in specific orientation at regulated densities on the surface of SVLS. The interior of pRBD and pHEL was filled with phosphate buffered saline (PBS). The other two sets: pRBD(iNA) and pHEL(iNA), schematically shown in Fig. 1C and D insets, are SVLS that not only display RBD or HEL on their surface, but also encapsulate nucleic acids inside these structures. All protein display was achieved through site-specific covalent conjugation on the lipid bilayer surface to ensure stability of the attachment with time (1, 2, 13). No proteins other than RBD or HEL were present in these structures. Fig. 1A through D show dynamic light scattering measurements of these

structures, with diameters around 120 nm, which is very close to that of HIV, influenza virus and SARS-CoV-2 (22-24). Fig. 1E shows a representative epi-fluorescence image of individual pRBD(iNA) stained by a fluorescent RBD-specific Fab (Fig. S1). We determined the average number of antigenic molecules per structure, termed epitope density (ED) herein, using both ensemble and single-molecule fluorescence techniques that we established previously (25-27). As shown in Table S1, we produced SVLS with a range of EDs for these structures that well covers the EDs observed for naturally occurring viruses (28, 29). As shown in Fig. 1F, the values of ED for pRBD(iNA) that we measured using a single-molecule fluorescence method (Fig. S1) overall agreed with ED values from ensemble-based measurement, even at low EDs. This is very important for the current study to identify the minimal structures of viruses for potent nAb induction, especially when we intend to assess the impact of just a few molecules of Ag per SVLS on B cell antibody production.

Most viruses infect their hosts through peripheral routes (30). To simulate a natural viral infection using SVLS, we delivered a submicrogram dose of Ag into mice through subcutaneous injection of SVLS. Subcutaneous injection allows viral collection by the initial lymphatics to encounter B cells in the lymph nodes (31). A submicrogram dose of Ag is equivalent to picomoles of SVLS, which is a very low dose of Ag compared to those typically used in vaccines comprised of VLPs (15, 32) and computationally designed self-assembling protein nanomaterials (33); and comparable to the Ag dose used in ferritin nanoparticle immunization (16). Natural viral infection does not involve any conventional adjuvants such as alum. To mimic this aspect, throughout, all the injections were performed in the absence of any exogenous adjuvants. As a result, the injections only introduced the highly purified protein Ags and lipids for pRBD or pHEL, and the Ags, lipids and purified

nucleic acids for pRBD(iNA) or pHEL(iNA). Moreover, all the SVLS were sterile filtered through 0.45 µm membranes before injections.

Rapid induction of IgG by SVLS without iNA

To our surprise, we found that a single injection of pRBD or pHEL at submicrogram Ag dose and in the absence of iNA or any other adjuvants is sufficient to elicit a fast onset of Ag-specific IgG response in both C57BL/6 (B6) and BALB/c mice, provided that the ED on SVLS was above an apparent threshold. This is shown in Fig. 2A and 2B for various conditions that we tested using pRBD and pHEL, respectively. For both SVLS, the Ag-specific IgG could be detected as early as day 5 post injection (D5, circles), with stronger responses on Day 11 (D11, columns) (Fig. 2A-2B, Conditions 6 and 7). The Ag-specific IgG responses were absent in several controls including PBS (Condition 1), soluble proteins (sRBD or sHEL, Condition 2), or an admixture of soluble proteins and control SVLS without conjugated proteins on the surface or iNA (Condition 3). In fact, a dose escalation of either sRBD or sHEL by tenfold could not elicit any detectable Ag-specific IgG through the same procedure. The exquisite sensitivity of animals towards pRBD or pHEL suggests that there are distinct signalling mechanisms involved in the sensing of these particulate Ags (34). In fact, in vitro studies using the same system of pHEL revealed that these SVLS were over 1000-fold more potent than respective soluble proteins in activation of Ag-specific B cells (34). Fig. 2A and 2B also revealed apparent thresholds of ED for IgG induction by either pRBD or pHEL in B6 mice. At the same Ag dose, an ED less than 20 was not sufficient to induce an Ag-specific IgG above background for either pRBD or pHEL (Fig. 2A-2B, Conditions 4 and 5). The IgG response increased with increasing ED for both pRBD and pHEL above the respective thresholds. Importantly, the animal sera from pRBD

immunization as in Conditions 6 and 7 could partially neutralize HIV-1 pseudovirions (35) that displayed the cognate S protein of the SARS-CoV-2 *in vitro* (Fig. 2C), suggesting that the antibodies present in these sera would be functional *in vivo* to offer host some protection against infection of SARS-CoV-2, as early as D5 upon Ag exposure. For both pRBD and pHEL, this fast IgG response induced IgG1, IgG2b and IgG3 in B6 mice (Fig. 2D-2I), with very low or undetectable IgM or IgG2c (Fig. S2), which shows similarity to the subclasses of IgG induced in the context of live viral infections (8) yet distinct from those induced by the type II T-independent Ags (36). These results suggest distinct actions of these SVLS in triggering class-switch recombination of the Ag-specific B cells *in vivo*. The presence of the HEL-specific IgG in B6 mice is surprising because it is well established that the B6 strain is unresponsive to HEL due to its failure to generate a dominant MHC Class II determinant (37), which suggests that the initiation of the fast nAb response by these SVLS is independent of T cells. To test this, we immunized B6 mice that were deficient in both alpha beta and gamma delta T-cell receptors ($TCR^{-/-}$) (38) with either pRBD or pHEL. Statistical comparisons between Condition 7 (wild-type B6 or wtB6) and Condition 8 ($TCR^{-/-}$) for pRBD4 in Fig. 2A or between Condition 6 (wtB6) and Condition 8 ($TCR^{-/-}$) for pHEL3 in Fig. 2B for both D5 and D11 did not reveal significant differences (p-values>0.1 for all cases), suggesting that this IgG response was largely T-independent for both Ags. Furthermore, the nAb response was also observed in B6 mice that were deficient in MyD88 (39) ($MyD88^{-/-}$) (Condition 9 in Fig. 2). Comparisons with respective wtB6 mice for both D5 and D11 did not reveal significant differences between Condition 7 (wtB6) and Condition 9 ($MyD88^{-/-}$) for pRBD4 in Fig. 2A or between Condition 6 (wtB6) and Condition 9 ($MyD88^{-/-}$) for pHEL3 in Fig. 2B (p-values>0.1 for all cases). These data ruled out the possibility that endotoxin or nucleic acid contamination of the SVLS produced these T-independent nAb responses, and suggest that the oriented display of foreign Ags above a threshold ED on a

virion-sized liposome, alone, can provide a sufficient '*external*' signal to trigger a fast nAb response. And this antibody response is in the absence of Toll-like receptor signalling (40). Consistent with these results, our studies using the same system of pHEL on Ag-specific B cells *in vitro* revealed that pHEL alone, without any exogenous adjuvants, can trigger robust B cell proliferation and survival in the absence of MyD88, IRAK1/4 and CD40 ligation (34). Moreover, the IgG response induced by pRBD or pHEL was completely abrogated in B6 mice that were deficient in CD19 ($CD19^{-/-}$) (41) (Condition 10). CD19 is an important coreceptor on B cells (42). It lowers the threshold for B cell antigen receptor activation (43) and is essential for B cell responses to membrane-bound ligands (44). These data indicate that CD19 is required for B cell production of IgG in response to these SVLS in the absence of iNA *in vivo*.

Compared to wtB6 mice, BALB/c mice also mounted a similar nAb response on D5 after immunization with pRBD or pHEL (Fig. 2J circles): the sera from pRBD injected mice could neutralize pseudovirions *in vitro* (2). The IgG response induced IgG1, IgG2b and IgG3, with low or undetectable Ag-specific IgM or IgG2a (Fig. S3). The presence of these similarities with B6 suggests that the early nAb response is an immediate host response that is conserved in both strains of mice. However, the IgG response in BALB/c mice on D11 was much higher than those in wtB6 mice (Fig. 2J columns), due to a much stronger IgG1 response that dominated on D11 for both pRBD and pHEL (Fig. S3B and S3G), suggesting that there are major differences between the two mouse strains in the amplification of the nAb response beyond D5 after its initial activation.

To gain more insight into the differences between the two strains of mice in their responses to SVLS, we collected inguinal lymph nodes from both animals on D12 after a single injection

of pRBD and stained cells for identification by flow cytometry. As shown in Fig. 3A and Fig. 3D for $CD19^+$ gated live lymphocytes in wtB6 and BALB/c mice respectively, we could clearly identify $GL7^+$ cells induced by pRBD well above those from either PBS (Condition 1) or soluble protein (Condition 2) immunized controls (Fig. 3B, 3E) for both wtB6 and BALB/c mice. However, we noticed that BALB/c mice consistently had higher percentages of Ag-induced $GL7^+$ B cells than those in wtB6. Comparison between wtB6 and BALB/c mice using one-way ANOVA test for Condition 3 returned a p-value of 6.4×10^{-7} and a p-value of 2.3×10^{-4} for Condition 4 between wtB6 and BALB/c mice, indicating statistical significance of these differences. Within these $CD19^+GL7^+$ cells, we identified $CD38^-CD95^+$ populations that corresponded to germinal center (GC) B cells in both wtB6 and BALB/c mice (Q1 in Fig. 3C, 3F). Consistent with lower percentages of $GL7^+$ B cells, the number of GC B cells induced by pRBD was much lower in wtB6 than BALB/c mice (p-value = 7.7×10^{-5} from one-way ANOVA test, N=4) under the same set of conditions. These data confirmed that B cell responses were initiated in both strains of animals upon a single exposure to submicrogram dose of pRBD, but the responses beyond D5 were amplified very differently.

Rapid and potent induction of IgG by SVLS with various iNA

Neither pRBD nor pHEL have iNA in their interiors. To examine the impact of iNA with natural phosphodiester backbones on the above nAb response, we administered a single subcutaneous injection of pRBD(iNA) or pHEL(iNA) to mice at submicrogram Ag dose without the use of additional adjuvants. As shown in Fig. 4A and 4C for various conditions that we have tested for pRBD(iNA) and pHEL(iNA), we first measured the Ag-specific IgG responses in mice of B6 genetic backgrounds on both D5 (circles) and D11 (columns) post injection using ELISA. These conditions included controls, SVLS of different ED, different

iNA sequences in either wtB6 or various gene knockout mice, as listed on the right in Fig. 4A and 4C. Many of these conditions induced strong Ag-specific IgG as early as D5 post injection, resulting in ELISA OD450 values >2. For correct interpretation of the data, we thus determined IgG titers for most conditions, as shown in Fig. 4B and 4D for pRBD(iNA) and pHEL(iNA), respectively. First, we observed a strong synergy between ED and iNA for SVLS encapsulating DNA1, a 20-mer single-stranded DNA that harbors two unmethylated CpG dinucleotides but has an all-natural phosphodiester backbone (Materials and methods), as shown by Conditions 4 through 7 for both RBD and HEL. When compared to either pRBD or pHEL without iNA, the titers of the IgG induced by these SVLS with DNA1 in wtB6 were all 10- to 1000-fold higher on D5 (circles, Fig. 4B and 4D), with an even stronger response on D11 (squares). As demonstrated by several controls in Fig. 4A and 4C, the simultaneous presence of ED and iNA on the same SVLS was necessary for the strong and rapid responses observed. Condition 1 is an admixture of soluble proteins with DNA1. Condition 2 and 3 are admixtures of DNA1 and SVLS of different ED without iNA. Although unmethylated CpG DNA can activate Toll-like receptor 9 (TLR9) (45), neither Condition 1 nor Condition 2 elicited Ag-specific IgG. Condition 3 elicited Ag-specific IgG but these responses were within error identical to those induced by SVLS alone without iNA (Fig. 2A and 2B), with p-values of 0.663 and 0.847 for pRBD3 on D5 and D11 and p-values of 0.728 and 0.787 on D5 and D11 for pHEL3 from one-way ANOVA tests. As we demonstrated previously (1), when provided in a simple admixture, these nucleic acids of all-natural phosphodiester backbones were quickly degraded in biological milieu. In contrast, when encapsulated within SVLS, the lipid bilayer structures protected iNA from nuclease degradation, like those in enveloped viruses. Therefore, even nucleic acids of all-natural phosphodiester backbones can unleash potent activity in current setting, when delivered together with ED on the same structures. Although enhancement of IgG by TLR9 ligands has

been reported previously (46), our result here distinguishes itself in its low Ag dose and yet enormous and unprecedented synergy (amounts to 1,000-fold enhancement in titer).

Strikingly, we noticed that as low as a few molecules of Ag per SVLS were able to elicit these strong responses for both pRBD(DNA1) and pHEL(DNA1) (Fig. 4A-4D, Condition 4). These results are surprising because an ED less than 20 was not sufficient to elicit an Ag-specific IgG above background for either pRBD or pHEL without iNA (Fig. 2). These data thus reveal that it is the integrative signals from both ED and iNA *on individual SVLS* that set the threshold for the induction of IgG *in vivo*. This integrative signal required for IgG secretion can be achieved with ED alone, at the expense of a relatively high ED value (Conditions 6 and 7 in Fig. 2), or the collective signals from ED and iNA together. However, the potency of IgG induction by ED alone is much lower than ED and iNA together for both D5 and D11, as demonstrated by the differences in resulting IgG titers (Fig. 4B and 4D).

The synergy between ED and iNA as we described above was also observed for two other nucleic acids that we tested: DNA2 and RNA1 (Fig. 4A and 4C Condition 10 and 11). DNA2 is a 20-mer single-stranded DNA that harbors two unmethylated GpC dinucleotides but has all-natural phosphodiester backbone, which was usually used as a control for CpG-containing DNA. RNA1 is a 20-mer single-stranded RNA that is highly conserved among SARS-CoV-1, SARS-CoV-2 and MERS-CoV, and encodes motif V of an essential RNA helicase in these coronaviruses (21) (Materials and methods). Although the IgG response from pRBD(DNA2) or pHEL(DNA2) was weaker than that of pRBD(DNA1) or pHEL(DNA1) at similar ED, the presence of the CpG dinucleotide motif was not required to observe this synergy. For pRBD(DNA2), the responses on both D5 and D11 were significantly higher than those induced by pRBD3, an SVLS of similar ED but without iNA

(Fig. 2A Condition 6), with p-values of 0.0104 and 3.76e-4 from one-way ANOVA tests. For pHEL(DNA2), the responses on both D5 and D11 were also significantly higher than those induced by pHEL3, an SVLS of even higher ED but without iNA (Fig. 2B Condition 6), with p-values of 0.0494 and 0.0285 from one-way ANOVA tests. For pRBD(RNA1) (Fig. 4B Condition 11), although the IgG titer on D5 was lower than that induced by pRBD(DNA1)4, an SVLS of similar ED with DNA1 (Fig. 4B Condition 7, p-value=2.88e-8 from one-way ANOVA test), the IgG titer on D11 was statistically identical (p-value=0.356 from one-way ANOVA test). Therefore, CpG DNA is not unique in its strong potency for the synergistic induction of Ag-specific IgG responses. A natural viral genomic sequence is sufficient to induce a strong and rapid IgG response that is comparable in its magnitude.

The use of B6 mice allows us to test several genetic conditions for mechanisms behind the enormous synergy between ED and iNA. First, the synergy was largely T-cell independent, as shown by the strong Ag-specific IgG observed in T-deficient mice for pRBD(DNA1) and pRBD(RNA1) (Fig. 4A-4B, Condition 8 and 12), pHEL(DNA1) and pHEL(RNA1) (Fig. 4C-4D, Condition 8 and 12). In contrast, the strong synergy required MyD88 or Toll-like receptors, as shown by the much attenuated IgG in mice deficient in MyD88 for pRBD(DNA1) or pHEL(DNA1) (Fig. 4A and 4C, Condition 9); and in mice deficient in Toll-like receptor 7 for pRBD(RNA1) or pHEL(RNA1) (Fig. 4A and 4C, Condition 13). However, in mice deficient in CD19, strikingly, the presence of DNA1 internal to these SVLS can elicit a fast and strong IgG response as early as D5 for both pRBD(DNA1) and pHEL(DNA1) (Fig. 4A and 4C, Condition 14, circles). On D11, the IgG titer induced by pRBD(DNA1)4 in CD19$^{-/-}$ mice (Fig. 4B Condition 14) was as strong as that in wtB6 mice induced by the same agent at the same Ag dose (Fig. 4B Condition 7, p-value=0.356 from one-way ANOVA test). Likewise, the IgG titer induced by pHEL(DNA1)2 in CD19$^{-/-}$ mice

on D11 (Fig. 4D Condition 14) was statistically identical to that in wtB6 mice induced by the same agent at the same Ag dose (Fig. 4D Condition 5, p-value=0.537 from one-way ANOVA test). These results are in sharp contrast to the requirement of CD19 by either pRBD or pHEL for induction of IgG in the absence of iNA (Fig. 2A-2B, Condition 10), and reveal that the synergistic signal co-delivered by ED and iNA for B cell activation can be strong enough to activate Ag-specific B cells even in the absence of the coreceptor CD19. Independent of the results from Condition 4 in wtB6 mice (Fig. 4A and 4C), these results in $CD19^{-/-}$ mice once again demonstrate that it is the integrative signal from ED and iNA together *on individual SVLS* that set the threshold for the induction of Ag-specific IgG *in vivo*. This integrative signal can potently induce IgG at low ED even when high ED alone cannot.

We also compared the Ab responses induced by SVLS with iNA (SVLS(iNA) herein) to a commonly used bacteriophage VLP-based vaccine platform (14, 15). The strong IgG induced by SVLS(iNA) was comparable in titers to those elicited by RBD or HEL conjugated on bacteriophage Qβ VLPs at the same Ag dose, despite the complete absence of the bacteriophage Qβ coat proteins in these SVLS(iNA). This was shown by Condition 15 in Fig. 4A and 4B for a Qβ-RBD conjugate with an ED of 200 and Condition 15 in Fig. 4C and 4D for a Qβ-HEL conjugate with an ED of 10 in wtB6. One-way ANOVA tests on these titer values revealed that Qβ-RBD induced the same level of RBD-specific IgG titers on D5 as pRBD(DNA1)1 and pRBD(DNA1)2, which were lower than those for pRBD(DNA1)3 and pRBD(DNA1)4; and Qβ-RBD induced the same level of RBD-specific IgG titers on D11 as pRBD(DNA1)3 and pRBD(DNA1)4, which were higher than those for pRBD(DNA1)1 and pRBD(DNA1)2 (Table S2A). For HEL, Qβ-HEL induced the same level of HEL-specific IgG titers on D5 and D11 as all pHEL(DNA1) (Table S2B). Bacteriophage VLPs are known to display superior immunogenicity (14, 15). These results demonstrate that it is feasible to

elicit IgG responses of a similar magnitude to bacteriophage VLPs using highly purified components.

Can these IgG molecules neutralize cognate viral infectivity? As shown in Fig. 4E (Conditions 4-7, 10-11, the same set of conditions as in Fig. 4A), for ED's as low as 6, the strong IgG induced by pRBD(iNA) as early as D5 after injection can potently neutralize HIV-1 pseudovirions that display the cognate S protein of SARS-CoV-2 *in vitro*, with an even stronger potency on D11 after immunization. These strong neutralizing activities were obtained for all iNA sequences that we tested, suggesting a broad relevance of these results to understanding viral immunogenicity. We noted that even in the absence of T cells, this nAb response was strong enough to potently neutralize cognate virions *in vitro* (Conditions 8 and 12 in Fig. 4E). These results are fully consistent with live viral infection literature showing potent nAb response in the absence of $CD4^+$ T cells (5, 8-10). Yet the data herein reveal that live infection is not required to mount a fast and potent nAb response; all that is needed are the key *external* signals common to viral infection: ED and iNA in the context of a *minimal structures of viruses* presented by SVLS. This fast and potent nAb response was also mounted in $CD19^{-/-}$ mice (Condition 14 in Fig. 4E), confirming that the coreceptor CD19 is not required for a potent nAb response, and that the integrative signals from ED and iNA on SVLS can be strong enough to overcome the apparent deficiency in CD19.

Like we observed in the B6 background, strong and fast IgG responses were also induced by SVLS(iNA) in BALB/c mice as early as D5. As shown in Fig. 4F, BALB/c mice mounted strong IgG responses towards pRBD(DNA1) of varied ED (Fig. 4F left, Conditions 4-7) with comparable magnitudes to B6 on both D5 and D11. Likely due to the available T cell help in BALB/c mice for HEL, the IgG responses towards pHEL(DNA1) of varied ED in BALB/c

mice were even stronger on D11 than those in wtB6 (Fig. 4F right, Conditions 5-7), indicated by one-way ANOVA tests on these titer values (Table S3). Therefore, a nAb response was robustly initiated upon a single exposure to a submicrogram dose of Ag on SVLS(iNA) in the absence of any other adjuvants in both strains of mice. The similar magnitudes of these responses between B6 and BALB/c mice suggest that this rapid and strong IgG secretion in response to these minimal structures of viruses is conserved between the two strains. Moreover, for both RBD and HEL, these responses induced by SVLS(iNA) could be quantitatively compared to those induced by either Qβ-RBD (Fig. 4F left, Condition 15) or Qβ-HEL conjugate (Fig. 4F right, Condition 15) at the same Ag dose in BALB/c mice. In contrast to bacteriophage Qβ VLPs that have multiple viral components (14), only three biochemical ingredients are needed to reconstitute such a response of similar magnitude: one foreign protein, iNA and lipids.

For both pRBD(iNA) and pHEL(iNA) in wtB6, the strong IgG response induced IgG1, IgG2b, IgG2c and IgG3, with IgG2c being the dominant subclass for almost all the SVLS(iNA) (Fig. 4G through 4N). Analogous to wtB6, the IgG response in BALB/c induced IgG1, IgG2a, IgG2b, and IgG3, with IgG2a being the dominant subclass (Fig. S4) (47). All iNA, including DNA1, DNA2 and RNA1, induced IgG2c in B6 genetic background (Fig. 4I and 4M), which was in sharp contrast to the undetectable IgG2c upon pRBD or pHEL immunization without iNA (Fig. S2B and S2D). Therefore these SVLS(iNA) can induce all the IgG subclasses known in mice, in the absence of live infection or any other adjuvants. Notably, incorporation of iNA lowers the ED thresholds for each IgG subclass. For SVLS without iNA, BALB/c mice mounted a stronger IgG1 response than wtB6 on D11 (Fig. S3). With iNA, the level of IgG1 is now comparable between the two strains particularly for RBD on both D5 and D11 (Fig. 4G, Fig. S4A and Table S4 for one-way ANOVA tests).

Moreover, the comparison between SVLS(iNA) and Qβ-conjugated Ags reveals that Qβ was a stronger inducer of IgG1 after D5 of immunization in both wtB6 (Fig. 4G and 4K, Condition 15) and BALB/c mice (Fig. S4A and S4E, Condition 6), although IgG1 is not the dominant IgG subclass induced by SVLS(iNA). One possibility among others for this difference is the presence of multiple copies of the bacteriophage coat protein in Qβ VLPs, a foreign protein that is known to recruit T cell help in wtB6 (13). Compared to the strong Ag-specific IgG response, the IgM response induced by the SVLS(iNA) or Qβ conjugates remained low overall in both B6 and BALB/c mice and dropped substantially on D11 for both RBD and HEL-conjugated Ags. (Fig. S5).

Discussion

In summary, we have discovered a mechanism for potent induction of neutralizing IgG by the minimal structures of enveloped viruses in mice. The IgG titers from this mechanism can exceed those produced by the well-established bacteriophage VLPs at the same Ag dose. This mechanism does not require any active viral replication or any other components. The minimal structure for potent nAb induction involves just a few molecules of surface antigen [$\leq (5 \pm 1)$] with internal nucleic acids in a virion-sized sphere, all of which are commonly found in naturally occurring viruses. This response as observed for two completely unrelated protein Ags on SVLS with RNA or DNA of different sequences but all-natural phosphodiester backbones suggests a broad relevance of the current findings for understanding viral immunogenicity and the mechanisms of nAb responses in mice.

Studies using inactivated viruses have established the significance of Ag repetitiveness for the induction of nAbs upon viral infection (3, 12). However, the presence of multiple

components in naturally occurring viruses renders it challenging to decipher the precise biochemical and biophysical signals from viral infections that initiate a nAb response. Using a set of SVLS that we constructed with highly purified biochemical ingredients, we have identified the minimal set of external signals from a virion that can robustly initiate antiviral IgG response *in vivo*. This IgG response is characterized by a fast onset of T-independent IgG of different subclasses and the ability to potently neutralize cognate virions. This system recapitulates several key features of the nAb response to live viral infections and therefore suggests a common mechanism for their induction.

Biochemically, only two ingredients are required to initiate a neutralizing IgG response (Fig. 2). The oriented display of viral surface proteins above a threshold ED on a virion-sized sphere is sufficient to serve as a stand-alone 'danger' signal to trigger an IgG response in the absence of cognate T cell help or Toll-like receptor signalling. Consistent with this, *in vitro* studies using the same system of pHEL demonstrated that these SVLS without iNA could activate the NF-κB signalling pathway in Ag-specific B cells independently of MyD88, IRAK1/4 and CD40 ligation (34). However, high ED is necessary to induce IgG *in vivo* in the absence of effective iNA signals (Fig. 2). Let it alone, high repetitiveness only has modest effects on nAb induction as compared to the minimal structures of viruses presented by SVLS(iNA), and the potency of this induction depends on mouse strains (Fig. 2). In contrast, the presence of iNA can substantially lower the threshold of ED for IgG induction. The sum signal of ED and iNA integrated by the Ag-specific B cells is also more potent than ED alone for the induction of nAbs. In the presence of iNA, both B6 and BALB/c mice mounted strong nAb responses of comparable magnitudes, suggesting that this is an evolutionarily conserved mechanism. The speed together with the magnitude of this response is largely independent of T cells, affording the host with a mechanism of fast and strong nAb

response that would be crucial for antiviral defense. This mechanism explains the induction of protective nAbs observed in live viral infections that do not require somatic hypermutation or affinity maturation (48). In the current study, this nAb response was initiated by SVLS at submicrogram Ag dose (picomoles of particles) upon a single exposure to the animal host in the absence of any other adjuvants. In the absence of iNA, the oriented display of proteins above a threshold ED on a virion-sized sphere can induce IgG1, IgG2b and IgG3 in both wtB6 and BALB/c mice. In the presence of iNA, IgG2a/2c was also induced. Thus, neither live infection nor any other adjuvants are necessary to initiate these class switches, although live viral infection can provide more sustained doses of these structures for nAb induction before the infection comes to an end.

The precise signal transduction pathways that allow the immune system to sense the minimal structures of viruses remain to be defined, but they must involve the collection of these structures into a single antigen-specific B cell for the activation of both B cell antigen receptors and Toll-like receptors therein, in the absence of cognate T cell help. It is highly likely that B cells use a signalling mechanism that is distinct from that for soluble antigens to sense these structures. For example, we show that pHEL can activate Ag-specific B cells through evasion of Lyn-dependent inhibitory pathways to initiate proliferation, which is in sharp contrast to the engagement of these inhibitory pathways by sHEL (34). On the other hand, because this general mechanism is so potent in nAb induction, viruses that are known to co-evolve with their hosts may evolve to encode virulence factors to antagonize this mechanism. The data in the current study suggest that this mechanism for the initiation of a nAb response is conserved between two different strains of mice: wtB6 and BALB/c.

The potency of the IgG response triggered by SVLS(iNA) can be compared to that of well-established bacteriophage VLPs, suggesting that the superior immunogenicity of VLPs may be reconstituted using highly purified components. Current study also reveal that other components present in bacteriophage VLPs can augment IgG1 production after the nAb response has been initiated. It's important to note that, in addition to binding rates, an IgG's potency for neutralizing viral infectivity is also influenced by the virus' ED. Specifically, the ED of the virus can impact the stability and effectiveness of bivalent binding by the IgG, which is more effective than monovalent binding (28). Finally, the SVLS as we used here in mice may be useful for studies in other mammalian species for a broader understanding of viral immunogenicity. The entirely synthetic nature of SVLS is useful for vaccine design, formulation and regulatory approval. The ability to induce potent nAb response without CD19 (Fig. 4) would be useful for patients who suffer from antibody-deficiency syndrome due to mutations in the *CD19* gene (49). The use of nucleic acids with native phosphodiester backbones without the need for nuclease-resistant phosphorothioate could substantially reduce the cost of vaccine manufacture.

MATERIALS AND METHODS

Synthesis of SVLS

All SVLS used throughout this study were prepared following protocols we published previously (1, 2, 13). These SVLS were constructed using nonimmunogenic lipids, with phosphatidylcholine and cholesterol comprising ≥ 99% of all lipids. These structures display protein antigens (Ags) of choice in a specific orientation on their surfaces with a regulated ED that quantitatively mimics the surface of naturally occurring viruses (28, 29) (Fig. 1). The HEL recombinant protein used in this study contains two site-directed mutations at R73E and D101R and was overexpressed in *E. coli* and purified to >95% purity following our established protocols (1). The SARS-CoV-2 RBD recombinant protein used in this study was overexpressed using 293F cells and also purified to >95% purity following our established protocols (2). DNA1, DNA2 and RNA1 were custom synthesized by IDT. The sequence of DNA1 is as follows, 5'-TCCATGA<u>CG</u>TTCCTGA<u>CG</u>TT-3'. The sequence of DNA2 is as follows, 5'-TCCATGA<u>GC</u>TTCCTGA<u>GC</u>TT-3'. The sequence of RNA1 is as follows, 5'-ACUGUUGAUUCAUCACAGGG-3'. Epitope density (ED) was quantified using methods that we established previously (1, 2, 13, 25) that were also validated by single-molecule fluorescence techniques (Fig. S1) that were developed and established in house (26, 27). For SVLS with iNA, the average number of internal nucleic acids (iNA) molecules per SVLS was also quantified using methods that we established previously (1, 2). Control SVLS had no surface protein conjugation nor internal encapsulated agents. Particle size was measured using a Malvern Zetasizer Nano ZSP at 20°C.

Conjugation of RBD or HEL to bacteriophage Qβ virus-like particles (VLPs)

The bacteriophage Qβ VLPs were prepared as described (50). The purified RBD or HEL recombinant proteins, which each contained a single reactive cysteine near their respective C-terminus, were conjugated to the surface of the VLPs using the heterobifunctional crosslinker Succinimidyl-6-[(β-maleimidopropionamido)hexanoate] (SMPH). Briefly, the VLPs were first derivatized with SMPH at a 10-fold molar excess of SMPH over Qβ coat protein. The mixture was incubated at 22°C for two hours and the excess crosslinker was removed by centrifugation at 4°C in an Amicon Ultra-4 centrifugal unit with a 100 kD cutoff. The RBD or HEL protein was then added to the derivatized VLPs and the mixture was incubated at 4°C overnight for RBD or at 20°C for 1 hour for HEL. Free proteins were then removed by centrifugation at 4°C in an Amicon Ultra-4 centrifugal unit with a 100 kD cutoff. The quantity of conjugated proteins was assessed using a denaturing polyacrylamide gel based on the intensity from silver staining in comparison with a standard curve obtained from the same gel.

Mice immunizations

All animal procedures were approved by the University of Michigan Animal Care and Use Committee. Female C57BL/6 or BALBc/J mice (8 weeks, Jackson Laboratory) were used for immunizations. Prior to inoculation, all injection samples were filtered through 0.45 µm pore size membrane to eliminate potential microbial contamination. 100 µL samples at a dose between 0.1 and 0.48 µg of respective protein Ags were injected into each mouse subcutaneously, 50 µL in each flank. Throughout the entire study, no adjuvants other than the SVLS were administered unless otherwise noted and only a single injection was administered throughout. Mouse blood was collected submentally using Microvette serum collection tubes (Sarstedt) three days before the first injection, and 5 days thereafter

following specified blood collection schedules. The sera were harvested by centrifugation at 10,000 g for 5 minutes, aliquoted and immediately frozen and stored at -80°C.

Four strains of gene knockout mice were purchased from Jackson Laboratory: $Tcrb^{tm1Mom}$/ $Tcrd^{tm1Mom}$ (#002122) ($TCR^{-/-}$ herein) was deficient in both alpha beta and gamma delta T-cell receptors (38). $Myd88^{tm1.Defr}$ (#009088) ($MyD88^{-/-}$ here in) encodes a deletion of exon 3 of the myeloid differentiation primary response gene 88 (39). $Cd19^{tm1(Cre)Cgn}$ (#006785) ($CD19^{-/-}$ herein) has a Cre recombinase gene inserted into the first exon of the CD19 gene thus abolishing CD19 gene function (41). $Tlr7^{tm1Flv}$ (#008380) ($TLR7^{-/-}$ herein) has a segment of exon 3 of the Toll-like receptor 7 gene replaced by a lacZ gene and a loxP-flanked neomycin resistance cassette thus abolishing the function of Toll-like receptor 7 (51). Gene knockout mice were housed in a germ-free environment and immunization protocols were carried out as described above.

Enzyme-Linked Immunosorbent Assay (ELISA)

Blood serum was tested by ELISA in order to quantitate Ag-specific IgG responses to various immunizations. 96-well plates (Nunc MaxiSorp, Invitrogen) were coated overnight at 4°C with either 200 ng of sHEL or 320 ng of sRBD per well in PBS. After blocking with 1% Bovine Serum Albumin (BSA, Fisher) in PBS, mouse sera of specified dilution factors were added to each well for incubation at 22°C for 2 hours. After three washes using PBS with 0.05% Tween 20, secondary goat anti-mouse IgG Fc-HRP antibody (# 1033-05, SouthernBiotech) was added in blocking buffer at 1:6000 dilution and incubated for 1 hour at 22°C. Following three washes, 100 µL of substrate 3,3',5,5'-Tetramethylbenzidine (Thermo Scientific) was added to each well and incubated in the dark for 10 minutes. The reaction

was stopped by addition of 100 µL 2M sulfuric acid in each well. The optical density of each well at 450nm was measured using a microplate reader (Bio-Tek Synergy HT). All the OD values reported were background subtracted by comparison between two wells that were coated with soluble protein and PBS, respectively. To determine the level of Ag-induced IgM in mice upon immunization by various agents, we used the following secondary antibody during ELISA: goat anti-mouse IgM HRP antibody (#1021-05, SouthernBiotech).

To determine the titers of Ag-specific IgG, we used a serial dilution of serum (from 1:100 dilution to 1:10,000,000 by a dilution factor of 10) for ELISA with the sHEL or sRBD protein. Cutoff values were calculated using the following equation as reported (52): Cutoff = $\bar{X} + SD \cdot f$, where $\bar{X}$ and SD are the mean and standard deviation of control well OD reading values, f is the standard deviation multiplier corresponding to different confidence levels. Specifically in our assays, f = 2.631 when the number of control wells was 4 and the confidence level was 95%. The titer value was determined as the highest dilution factor of the serum that still yielded an OD450 value higher than the above cutoff value in ELISA.

To determine the subclasses of IgG antibodies elicited in mice upon immunization by various agents, we used the following secondary antibodies during ELISA: goat anti-mouse IgG1 HRP antibody (#1071-05, SouthernBiotech), goat anti-mouse IgG2a HRP antibody (#1081-05, SouthernBiotech), goat anti-mouse IgG2b HRP antibody (#1091-05, SouthernBiotech), goat anti-mouse IgG2c HRP antibody (#1078-05, SouthernBiotech), and goat anti-mouse IgG3 HRP antibody (#1101-05, SouthernBiotech).

Preparation of HIV-1 virions pseudotyped with SARS-CoV-2 envelope

The HIV-1 pseudotyped with SARS-CoV-2 envelope was prepared following the published protocols (53) but with modifications. Briefly, HEK 293T/17 cells (ATCC, Manassas, VA) were cultured at 37°C with 5% CO_2 in DMEM supplemented with 10% FBS (HyClone Laboratories, Logan, UT). 10^6 293T cells in a 2-mL culture volume were seeded overnight in a 35-mm dish before transfection using the TransIT LT-1 transfection reagent (Mirus Bio, Madison, WI). For each dish, 2 μg of the provirus-containing plasmid pNL4-3 luc R^-E^- (54) (ARP-3418, NIH AIDS Research and Reference Reagent Program) was used to make the transfection reagent mixture, together with 1 μg of envelope expression plasmid pcDNA3.1 SARS-CoV-2 S D614G (53). The plasmid pcDNA3.1 SARS-CoV-2 S D614G was a gift from Jeremy Luban (Addgene plasmid # 158075 ; http://n2t.net/addgene:158075 ; RRID:Addgene_158075). The RBD amino acid sequence 328-537 encoded in this plasmid is identical to the sequence of RBD that we studied here. The transfection reagent mixture was incubated at room temperature for 15 min before drop wise addition to the culture medium, as we did previously (55). At 6 hours post transfection, the culture medium together with the transfection reagents was replaced with fresh complete medium and the incubation was continued at 37°C with 5% CO_2. At 48 hours post transfection, the entire culture medium containing single-cycle HIV-1 viruses was collected and filtered through a 0.45-μm syringe filter (Millex-HV PVDF, Millipore). The filtrate was then aliquoted on ice, flash-frozen in liquid nitrogen and stored in a -80°C freezer. The concentration of virion particles was quantitated using a HIV-1 p24 ELISA kit (CAT#XB-1000, XpressBio) as we described previously (55).

Virion neutralization assay

Virion neutralization assay follows the protocols we established previously but with important modifications (55). HIV-1 virions pseudotyped with SARS-CoV-2 envelope containing 9 ng of HIV-1 p24 were incubated with various mouse sera at 37°C for one hour, and then diluted with complete medium by 8-fold in volume for the sera to initiate infection of Huh-7.5 cells at 37°C for 2 hours. At the end of 2 hours, fresh medium was added to each well in a 24-well plate and the incubation was continued at 37°C with 5% CO_2. Luciferase activity was measured 48 hours after infection. Briefly, the culture medium was removed and replaced with 100 μL of complete medium. 100 μL of Bright-Glo™ reagent (CAT#E2610, Promega) that was just warmed to room temperature was then added to each well. The cells were incubated for three minutes at room temperature to allow cell lysis. After three minutes, 100 μL of lysate from each well was transferred to a single well in a 96-well black microtiter plate (Costar). Luminescence was measured using a Synergy™ HT multi-mode plate reader (BioTek Instruments Inc., Vermont) and background luminescence was subtracted using Huh-7.5 cells without virus infection. For comparison among different immunization groups in Fig. 2C and Fig. 4E, the luminescence readings for cells incubated with sera from PBS-injected mice was set as 100%. The luminescence readings from other groups were all normalized based on this and plotted as a percentage of remaining infectivity.

Flow cytometry analysis of mouse inguinal lymph nodes

On Day 12 following mouse inoculation with various agents, mice were euthanized by CO_2 inhalation followed by rapid dissection of the inguinal lymph nodes. The lymph nodes were minced on ice and a cellular suspension was separated from tissue using a 40 μm cell strainer. Single cell suspensions of mouse lymph node cells were first incubated with rat anti-mouse CD16/CD32 (BD Pharmingen #553142) on ice for 15 min, followed by incubation with

fluorophore-conjugated antibodies on ice covered by aluminum foil. The cells were washed twice with 200 µL of FACS buffer, resuspended in FACS buffer, and fixed in the presence of 2% PFA at 22°C for 1 hour before data acquisition on a Miltenyi MACSQuant VYB flow cytometer equipped with 3 spatially-separated lasers (405, 488 and 561 nm) and 10 detection channels. A minimum of 100,000 events were collected for all experiments. The fluorophore-conjugated antibodies were pacific blue rat anti-mouse CD19 (Biolegend #115526), FITC rat anti-mouse GL7 antigen (Biolegend #144603), PE anti-mouse CD38 (Biolegend #102707), and APC anti-mouse CD95 (Biolegend #152603). The data were analyzed using FlowJo (BD).

Statistical analysis

Statistical analysis was carried out using the Statistics toolbox in MATLAB (Mathworks, MA) or the statistical analysis tools in OriginLab (Northampton, MA). A comparison of two independent variables was carried out using a two-sample T-test. Data sets with more than two independent variables were analyzed using a one-way analysis of variance as indicated. P-values less than 0.05 were considered statistically significant. The details of all statistical analysis are described explicitly throughout the paper. All data points in figures were reported as mean ± standard error unless otherwise noted.

Data availability

All data are available in the main text or the suporting figures and tables.

References

1. W. Y. Wholey *et al.*, Synthetic Liposomal Mimics of Biological Viruses for the Study of Immune Responses to Infection and Vaccination. *Bioconjug Chem* **31**, 685-697 (2020).
2. W. Y. Wholey, S. T. Yoda, W. Cheng, Site-Specific and Stable Conjugation of the SARS-CoV-2 Receptor-Binding Domain to Liposomes in the Absence of Any Other Adjuvants Elicits Potent Neutralizing Antibodies in BALB/c Mice. *Bioconjug Chem* **32**, 2497-2506 (2021).
3. M. F. Bachmann, R. M. Zinkernagel, Neutralizing antiviral B cell responses. *Annu Rev Immunol* **15**, 235-270 (1997).
4. J. H. Lam, N. Baumgarth, The Multifaceted B Cell Response to Influenza Virus. *J Immunol* **202**, 351-359 (2019).
5. E. Szomolanyi-Tsuda, R. M. Welsh, T-cell-independent antiviral antibody responses. *Curr Opin Immunol* **10**, 431-435 (1998).
6. L. Hangartner, R. M. Zinkernagel, H. Hengartner, Antiviral antibody responses: the two extremes of a wide spectrum. *Nat Rev Immunol* **6**, 231-243 (2006).
7. M. K. Slifka, R. Ahmed, Long-term humoral immunity against viruses: revisiting the issue of plasma cell longevity. *Trends Microbiol* **4**, 394-400 (1996).
8. B. O. Lee *et al.*, CD4 T cell-independent antibody response promotes resolution of primary influenza infection and helps to prevent reinfection. *J Immunol* **175**, 5827-5838 (2005).
9. N. Juleff *et al.*, Foot-and-mouth disease virus can induce a specific and rapid CD4+ T-cell-independent neutralizing and isotype class-switched antibody response in naive cattle. *J Virol* **83**, 3626-3636 (2009).
10. L. C. Wang *et al.*, CD4 T-cell-independent antibody response reduces enterovirus 71 lethality in mice by decreasing tissue viral loads. *Clin Dev Immunol* **2012**, 580696 (2012).
11. I. J. Amanna, N. E. Carlson, M. K. Slifka, Duration of humoral immunity to common viral and vaccine antigens. *N Engl J Med* **357**, 1903-1915 (2007).
12. M. F. Bachmann *et al.*, The influence of antigen organization on B cell responsiveness. *Science* **262**, 1448-1451 (1993).
13. Z. Chen *et al.*, Self-Antigens Displayed on Liposomal Nanoparticles above a Threshold of Epitope Density Elicit Class-Switched Autoreactive Antibodies Independent of T Cell Help. *J Immunol* **204**, 335-347 (2020).
14. M. F. Bachmann, G. T. Jennings, Vaccine delivery: a matter of size, geometry, kinetics and molecular patterns. *Nat Rev Immunol* **10**, 787-796 (2010).
15. B. Chackerian, D. R. Lowy, J. T. Schiller, Conjugation of a self-antigen to papillomavirus-like particles allows for efficient induction of protective autoantibodies. *J Clin Invest* **108**, 415-423 (2001).
16. M. Kanekiyo *et al.*, Self-assembling influenza nanoparticle vaccines elicit broadly neutralizing H1N1 antibodies. *Nature* **499**, 102-106 (2013).
17. N. P. King *et al.*, Computational design of self-assembling protein nanomaterials with atomic level accuracy. *Science* **336**, 1171-1174 (2012).
18. T. M. Allen, P. R. Cullis, Drug delivery systems: entering the mainstream. *Science* **303**, 1818-1822 (2004).
19. D. S. Watson, A. N. Endsley, L. Huang, Design considerations for liposomal vaccines: influence of formulation parameters on antibody and cell-mediated immune responses to liposome associated antigens. *Vaccine* **30**, 2256-2272 (2012).
20. N. Pardi, M. J. Hogan, F. W. Porter, D. Weissman, mRNA vaccines - a new era in vaccinology. *Nat Rev Drug Discov* **17**, 261-279 (2018).
21. P. Zhou *et al.*, A pneumonia outbreak associated with a new coronavirus of probable bat origin. *Nature* **579**, 270-273 (2020).

22. A. Harris *et al.*, Influenza virus pleiomorphy characterized by cryoelectron tomography. *Proc Natl Acad Sci U S A* **103**, 19123-19127 (2006).
23. J. A. Briggs, T. Wilk, R. Welker, H. G. Krausslich, S. D. Fuller, Structural organization of authentic, mature HIV-1 virions and cores. *EMBO J* **22**, 1707-1715 (2003).
24. Z. Ke *et al.*, Structures and distributions of SARS-CoV-2 spike proteins on intact virions. *Nature* 10.1038/s41586-020-2665-2 (2020).
25. Z. Chen, J. J. Moon, W. Cheng, Quantitation and Stability of Protein Conjugation on Liposomes for Controlled Density of Surface Epitopes. *Bioconjug Chem* **29**, 1251-1260 (2018).
26. Y. Pang, H. Song, J. H. Kim, X. Hou, W. Cheng, Optical trapping of individual human immunodeficiency viruses in culture fluid reveals heterogeneity with single-molecule resolution. *Nat Nanotechnol* **9**, 624-630 (2014).
27. M. C. DeSantis, J. H. Kim, H. Song, P. J. Klasse, W. Cheng, Quantitative Correlation between Infectivity and Gp120 Density on HIV-1 Virions Revealed by Optical Trapping Virometry. *J Biol Chem* **291**, 13088-13097 (2016).
28. J. S. Klein, P. J. Bjorkman, Few and far between: how HIV may be evading antibody avidity. *PLoS Pathog* **6**, e1000908 (2010).
29. W. Cheng, The Density Code for the Development of a Vaccine? *J Pharm Sci* **105**, 3223-3232 (2016).
30. D. M. Knipe, P. M. Howley, *Fields virology* (Wolters Kluwer/Lippincott Williams & Wilkins Health, Philadelphia, PA, ed. 6th, 2013), pp. 2 volumes.
31. T. Junt *et al.*, Subcapsular sinus macrophages in lymph nodes clear lymph-borne viruses and present them to antiviral B cells. *Nature* **450**, 110-114 (2007).
32. A. F. Ochsenbein *et al.*, Correlation of T cell independence of antibody responses with antigen dose reaching secondary lymphoid organs: implications for splenectomized patients and vaccine design. *J Immunol* **164**, 6296-6302 (2000).
33. A. C. Walls *et al.*, Elicitation of Potent Neutralizing Antibody Responses by Designed Protein Nanoparticle Vaccines for SARS-CoV-2. *Cell* **183**, 1367-1382 e1317 (2020).
34. J. F. Brooks *et al.*, Molecular basis for potent B cell responses to antigen displayed on particles of viral size. *BioRxiv* https://doi.org/10.1101/2023.02.15.528761 (2023).
35. F. Schmidt *et al.*, Measuring SARS-CoV-2 neutralizing antibody activity using pseudotyped and chimeric viruses. *J Exp Med* **217** (2020).
36. H. Tesch, F. I. Smith, W. J. Muller-Hermes, K. Rajewsky, Heterogeneous and monoclonal helper T cells induce similar anti-(4-hydroxy-3-nitrophenyl)acetyl (NP) antibody populations in the primary adoptive response. I. Isotype distribution. *Eur J Immunol* **14**, 188-194 (1984).
37. I. S. Grewal, K. D. Moudgil, E. E. Sercarz, Hindrance of binding to class II major histocompatibility complex molecules by a single amino acid residue contiguous to a determinant leads to crypticity of the determinant as well as lack of response to the protein antigen. *Proc Natl Acad Sci U S A* **92**, 1779-1783 (1995).
38. P. Mombaerts *et al.*, Mutations in T-cell antigen receptor genes alpha and beta block thymocyte development at different stages. *Nature* **360**, 225-231 (1992).
39. B. Hou, B. Reizis, A. L. DeFranco, Toll-like receptors activate innate and adaptive immunity by using dendritic cell-intrinsic and -extrinsic mechanisms. *Immunity* **29**, 272-282 (2008).
40. A. L. Gavin *et al.*, Adjuvant-enhanced antibody responses in the absence of toll-like receptor signaling. *Science* **314**, 1936-1938 (2006).
41. R. C. Rickert, J. Roes, K. Rajewsky, B lymphocyte-specific, Cre-mediated mutagenesis in mice. *Nucleic Acids Res* **25**, 1317-1318 (1997).
42. R. C. Rickert, K. Rajewsky, J. Roes, Impairment of T-cell-dependent B-cell responses and B-1 cell development in CD19-deficient mice. *Nature* **376**, 352-355 (1995).
43. R. H. Carter, D. T. Fearon, CD19: lowering the threshold for antigen receptor stimulation of B lymphocytes. *Science* **256**, 105-107 (1992).

44. D. Depoil *et al.*, CD19 is essential for B cell activation by promoting B cell receptor-antigen microcluster formation in response to membrane-bound ligand. *Nat Immunol* **9**, 63-72 (2008).
45. H. Hemmi *et al.*, A Toll-like receptor recognizes bacterial DNA. *Nature* **408**, 740-745 (2000).
46. J. Eckl-Dorna, F. D. Batista, BCR-mediated uptake of antigen linked to TLR9 ligand stimulates B-cell proliferation and antigen-specific plasma cell formation. *Blood* **113**, 3969-3977 (2009).
47. A. Jegerlehner *et al.*, TLR9 signaling in B cells determines class switch recombination to IgG2a. *J Immunol* **178**, 2415-2420 (2007).
48. U. Kalinke *et al.*, The role of somatic mutation in the generation of the protective humoral immune response against vesicular stomatitis virus. *Immunity* **5**, 639-652 (1996).
49. M. C. van Zelm *et al.*, An antibody-deficiency syndrome due to mutations in the CD19 gene. *N Engl J Med* **354**, 1901-1912 (2006).
50. K. K. Van Rompay *et al.*, A vaccine against CCR5 protects a subset of macaques upon intravaginal challenge with simian immunodeficiency virus SIVmac251. *J Virol* **88**, 2011-2024 (2014).
51. J. M. Lund *et al.*, Recognition of single-stranded RNA viruses by Toll-like receptor 7. *Proc Natl Acad Sci U S A* **101**, 5598-5603 (2004).
52. A. Frey, J. Di Canzio, D. Zurakowski, A statistically defined endpoint titer determination method for immunoassays. *J Immunol Methods* **221**, 35-41 (1998).
53. L. Yurkovetskiy *et al.*, Structural and Functional Analysis of the D614G SARS-CoV-2 Spike Protein Variant. *Cell* **183**, 739-751 e738 (2020).
54. R. I. Connor, B. K. Chen, S. Choe, N. R. Landau, Vpr is required for efficient replication of human immunodeficiency virus type-1 in mononuclear phagocytes. *Virology* **206**, 935-944 (1995).
55. J. H. Kim, H. Song, J. L. Austin, W. Cheng, Optimized Infectivity of the Cell-Free Single-Cycle Human Immunodeficiency Viruses Type 1 (HIV-1) and Its Restriction by Host Cells. *PLoS One* **8**, e67170 (2013).

Acknowledgements:

This work is supported by NIH/NIAID grant 1R01AI155653-01A1 to WC and JZ. We thank Prof. Irina Grigorova for critical reading of the work during the early development of the manuscript. We thank Dr. Charlie Rice at Rockefeller University for the kind gift of Huh-7.5 cells. The following reagent was obtained through the AIDS Research and Reference Reagent Program, Division of AIDS, National Institute of Allergy and Infectious Diseases (NIAID), National Institutes of Health (NIH): pNL4-3.Luc.R-E- from Dr. Nathaniel Landau. The plasmid pcDNA3.1 SARS-CoV-2 S D614G was a gift from Dr. Jeremy Luban through Addgene.

Author contributions:

W.C. conceived and directed the project. W.W., A.R.M., S.Y., and B.C. prepared experimental materials. W.W., A.R.M., S.Y. and W.C. conducted the experiments. W.W., A.R.M., S.Y. and W.C. performed the analysis. W.W., A.R.M., B.C., J.Z. and W.C. wrote the paper.

Competing interests

W. Cheng has a patent pending on SVLS. B. Chackerian has equity in Flagship Laboratories 72. J. Zikherman is on the scientific advisory board for Walking Fish Therapeutics. No other disclosures were reported.

Materials and Correspondence to W.C.

Figures

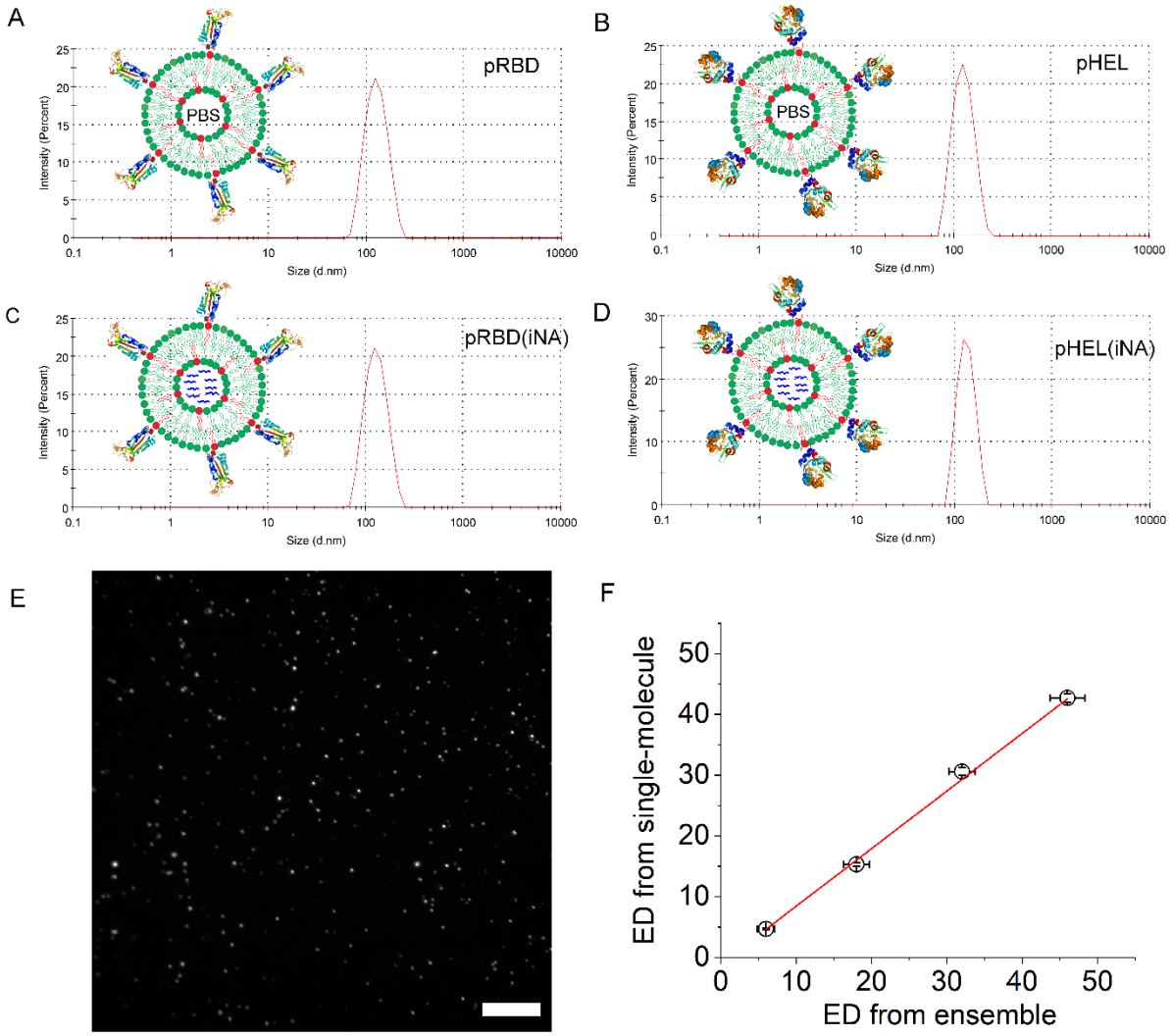

Fig. 1. Characterization of SVLS that quantitatively incorporate the common consensus features of enveloped viruses. (**A**) through (**D**): representative intensity distributions of particle sizes measured using dynamic light scattering for four types of SVLS, schematically shown as insets in each panel. The structure surface is conjugated with RBD (A, C) or HEL (B, D) site-specifically at regulated average spatial densities. The internal space of the structures is either PBS for investigation of ED in isolation (A, B) or loaded with nucleic acids to study the effects of iNA (C, D). The average diameters together with PDI values are 122 nm, 0.037 for a pRBD; 120 nm, 0.039 for a pHEL; 123 nm, 0.042 for a pRBD(DNA1); and 124 nm, 0.054 for a pHEL(DNA1). Cartoon insets adapted from (1, 2). (**E**) A representative epi-fluorescence image of individual SVLS on poly-L-lysine coated coverslip stained by a fluorescent Fab (Fig. S1). The scale bar represents 10 µm. (**F**) Correlation between ED measured using single-molecule fluorescence technique (Fig. S1) and ensemble technique for a set of pRBD(DNA1).

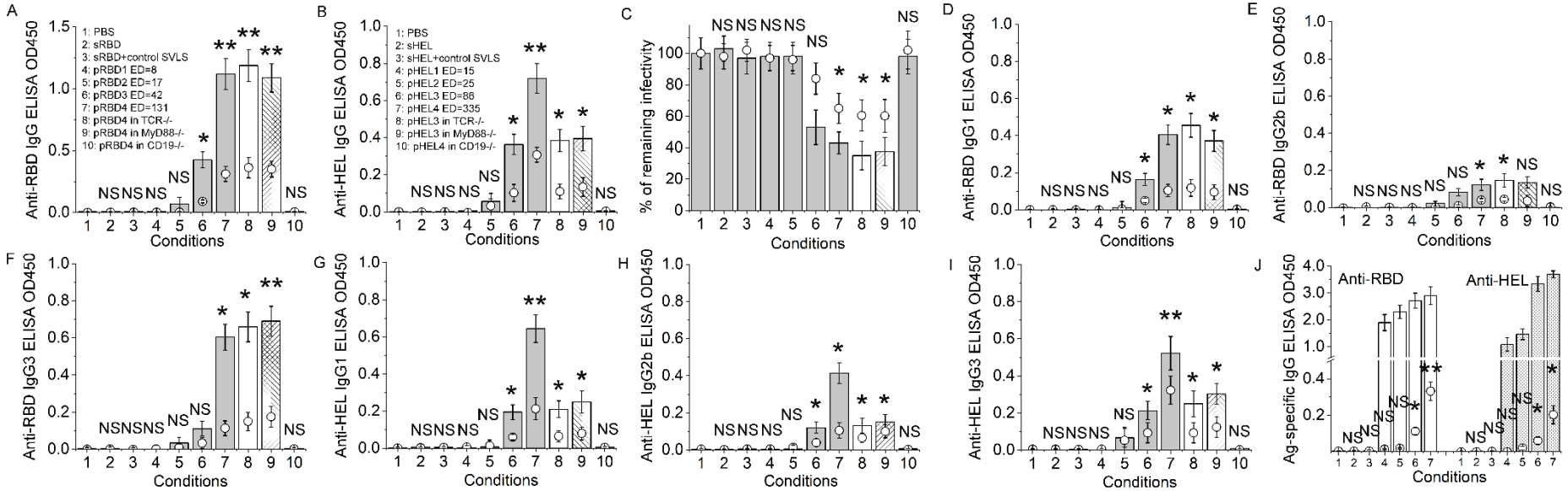

Fig. 2. Rapid nAb responses induced by SVLS without iNA. (**A**)(**B**) ELISA OD values for RBD-specific IgG (A) or HEL-specific IgG (B) in B6 genetic background after a single injection using various agents listed in the insets. (**C**) Neutralization of HIV-1 virions pseudotyped with SARS-CoV-2 S protein by mouse sera. (**D**) through (**I**): ELISA OD values for RBD- and HEL-specific IgG subclasses in (A) and (B). (**J**) ELISA OD values for RBD-specific IgG (left) or HEL-specific IgG (right) in BALB/c after a single injection using various agents listed in (A) and (B) insets. Throughout Fig. 2, data from D5 post immunization shown in circles and D11 shown in columns; sera were diluted 100-fold for all ELISA; the doses of RBD and HEL were 0.24 and 0.3 µg per animal, respectively for Conditions 2 through 10. The pairwise statistical difference between each condition and Condition 1 on Day 5 was determined by Student's T-test and shown using the following set of symbols; **: p-value < 0.01; *: p-value < 0.05; NS: not significant, p-value > 0.05. N=4.

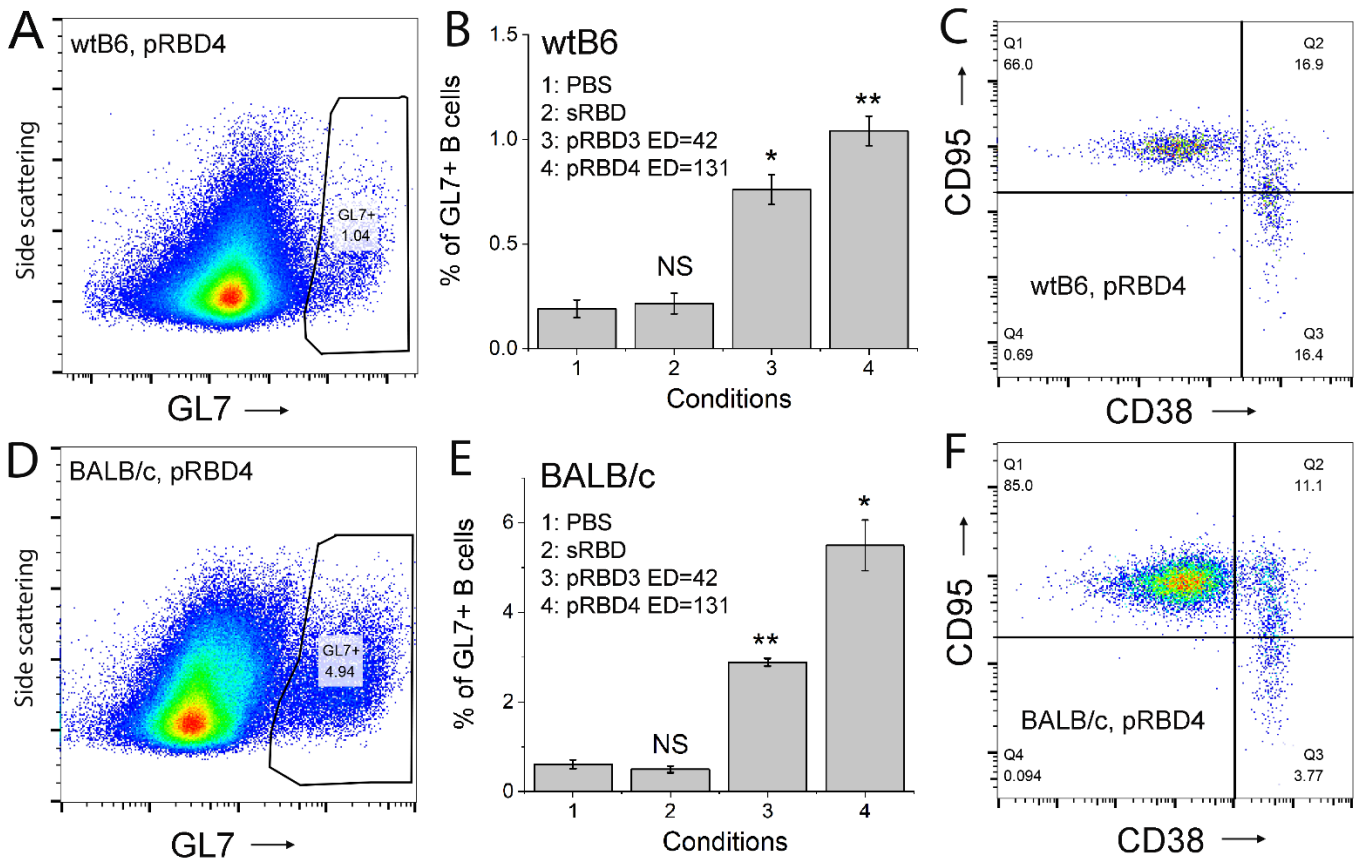

Fig. 3. Flow cytometry analysis of germinal center B cells from inguinal lymph nodes on Day 12 after injection with various reagents. (A) and **(D)**, cytograms showing $GL7^+$ B cells within live $CD19^+$ B cells after a single injection of pRBD4 in wtB6 (A, 198,981 events), and BALB/cJ (D, 164,697 events), respectively. (**B**) and (**E**), percent of $GL7^+$ B cells within live $CD19^+$ B cells after a single injection of various agents in wtB6 (B) and BALB/cJ (E) respectively, including PBS (Condition 1), soluble proteins (Condition 2), pRBD3 (Condition 3), or pRBD4 (Condition 4). PBS-injected mice were used as a reference to determine the pairwise statistical difference between data points by Student's T-test. The statistical difference was denoted using the same set of symbols as Fig. 2. N=4. (**C**) and (**F**), $CD38^-CD95^+$ germinal center

B cells, indicated by Q1 in Panel C (1,248 events) and F (6,931 events) and gated by $GL7^+$ $CD19^+$ live B cells from panel A and E, respectively. Throughout Fig. 3, the dose of RBD was 0.48 µg per animal for Conditions 2 through 4.

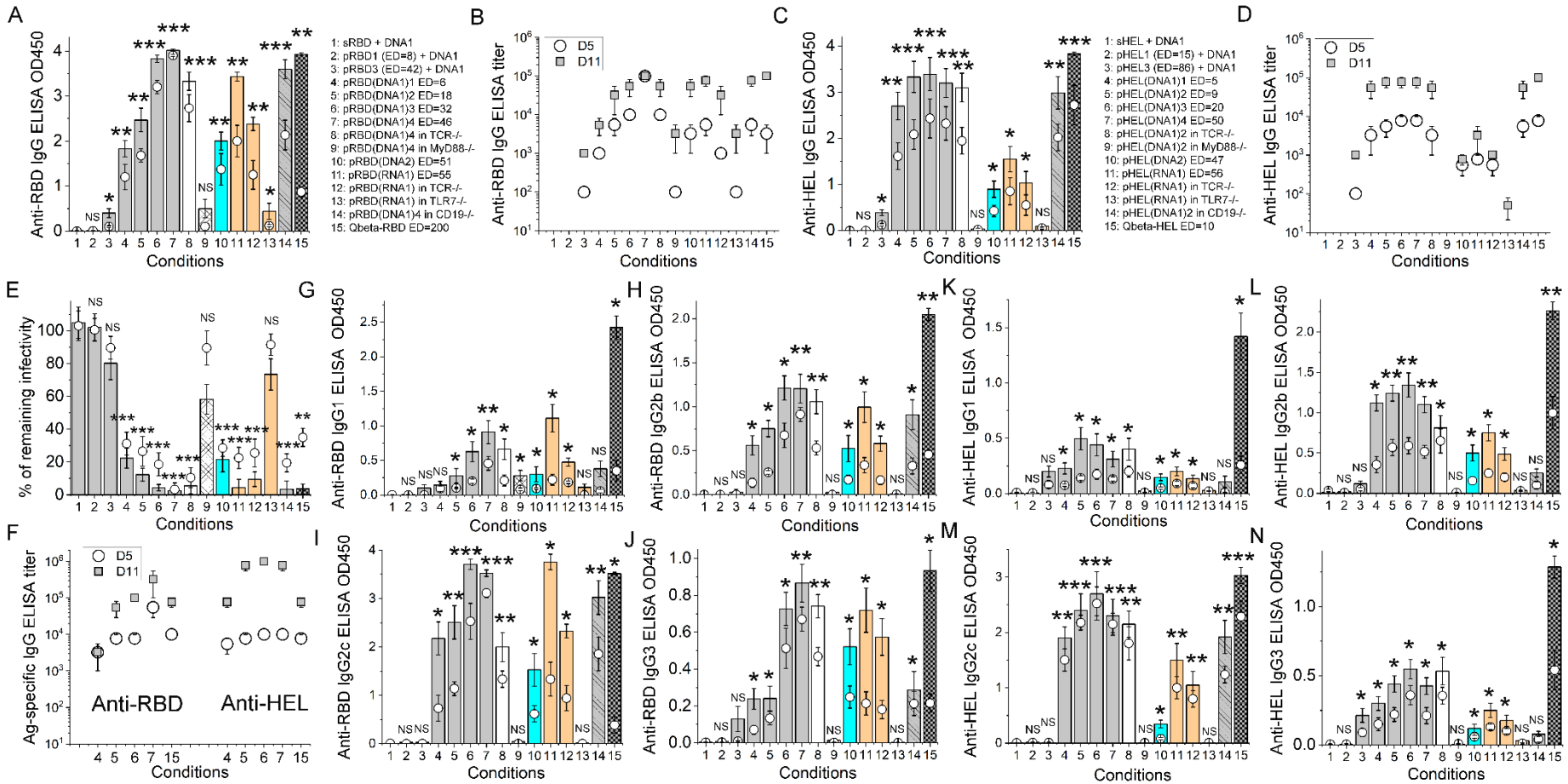

Fig. 4. Rapid nAb responses induced by SVLS with various iNA. (**A**) and (**C**) ELISA OD values for RBD-specific IgG (A) or HEL-specific IgG (C) in B6 genetic background after a single injection using various agents listed in the insets. (**B**) and (**D**) Titers for RBD-specific IgG (B) or HEL-specific IgG (D) measured for various conditions as in (A) and (C). (**E**) Neutralization of HIV-1 virions pseudotyped with SARS-CoV-2 S protein by mouse sera from various conditions in (A). (**F**) Ag-specific titer values for RBD-specific IgG (left) or HEL-specific IgG (right) in BALB/c after a single injection using agents #4, 5, 6, 7 and 15 as listed in (A) and (C) insets. (**G**) through (**N**): ELISA OD values for RBD-specific (G through J) and HEL-specific (K through N) IgG subclasses for sera from (A) and (C), respectively. Throughout Fig. 4, data from D5

post immunization shown in circles and D11 shown in columns or squares; sera were diluted 100-fold for all ELISA except titers; the doses of RBD and HEL were 0.24 and 0.1 µg per animal, respectively for Conditions 2 through 15; the pairwise statistical difference between each condition and Condition 1 on Day 5 was determined by Student's T-test and shown using the following set of symbols; ***: p-value < 0.001; **: p-value < 0.01; *: p-value < 0.05; NS: not significant, p-value > 0.05. N=4.

Supporting Information for

Initiation of neutralizing antibody response probed using synthetic virus-like structures

Wei-Yun Wholey[1†], Alexander R. Meyer[1†], Sekou-Tidiane Yoda[1], Bryce Chackerian[2], Julie Zikherman[3], Wei Cheng[1,4*]

[1]*Department of Pharmaceutical Sciences, 428 Church Street, University of Michigan, Ann Arbor, Michigan 48109, USA*

[2]*Department of Molecular Genetics and Microbiology, School of Medicine, University of New Mexico, Albuquerque, New Mexico 87131, USA*

[3]*Division of Rheumatology, Rosalind Russell and Ephraim P. Engleman Arthritis Research Center, Department of Medicine, University of California, San Francisco, California 94143 USA*

[4]*Department of Biological Chemistry, 1150 W. Medical Center Dr., University of Michigan Medical School, Ann Arbor, Michigan 48109, USA*

Correspondence to: chengwe@umich.edu

This PDF file includes:

Figs. S1 to S5

Tables S1 to S4

SI Referenes

Fig. S1. Characterization of RBD-conjugated SVLS using a single-molecule fluorescence approach.

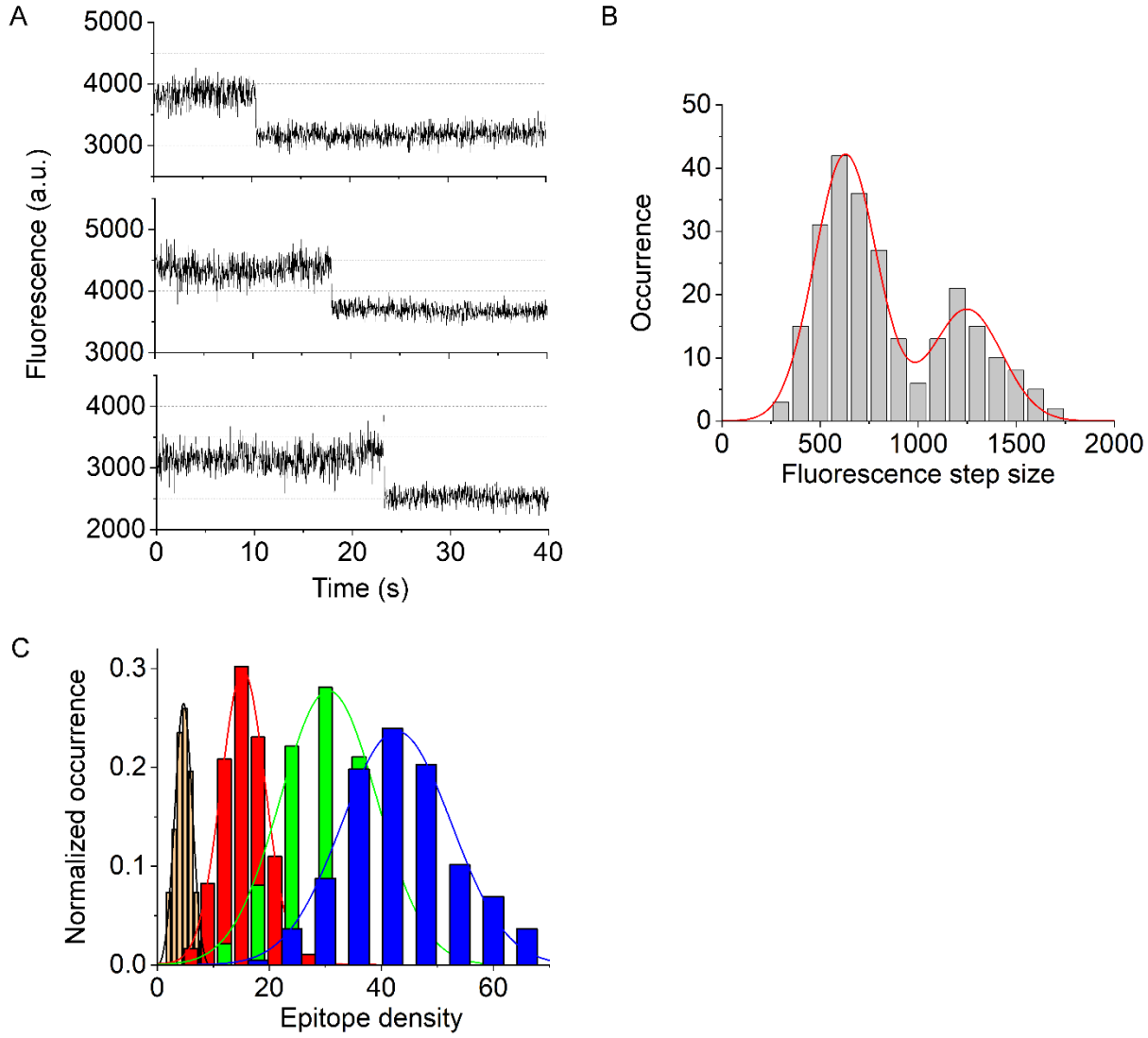

(**A**) Representative single-molecule fluorescence trajectories from Alexa-594 labeled RBD-specific Fab (Alexa-594-Fab). We prepared Alexa-594-Fab using a monoclonal IgG2a specific for SARS-CoV-2 RBD (Biolegend #944803, mAb1 herein). This high-affinity Fab allowed us to quantitate epitope density on individual SVLS conjugated with RBD, using single-molecule fluorescence techniques that we established previously (1-3). Briefly, the Fab was prepared from the IgG form of the antibody using a Pierce^{TM} Fab Micro preparation kit (ThermoFisher Scientific, CAT#44685) following manufacturer instructions. The purified Fab was then labeled using Alexa Fluor 594 succinimidyl NHS ester (ThermoFisher Scientific, CAT#A37572) following the protocol that we established previously (1). The labeling ratio between the dye and protein was determined to be 3.3 dye molecules per Fab based on single-molecule two-photon fluorescence measurement as we described previously (1). As shown in Fig. 1E in the main text, we deposited pRBD(DNA1)4 bound with Alexa-594-Fab on poly-L-lysine coated coverslips, and used epi-fluorescence imaging to directly visualize individual SVLS through excitation of the Alexa-594 fluorophore by a 592-nm laser. Individual SVLS showed up as bright spots in a dark background. Neither SVLS alone

nor free Alexa-594-Fab alone at the same concentrations yielded these bright spots under the microscope. Moreover, no fluorescent spots were visible when Alexa-594-Fab was incubated with control SVLS without RBD conjugation, confirming that these fluorescent spots were specific for SVLS conjugated with RBD but not protein aggregates. In order to determine the number of RBD molecules per SVLS, we chose to work at a laser power of 100 mW. This illumination condition allowed us to collect the initial fluorescence intensity from individual spots, and the constant illumination of the sample under this condition also allowed us to observe the photobleaching of individual fluorophores with time. As shown in Fig. S1A, these photobleaching events display a hallmark feature of 'steps', where the fluorescence persists for a finite time followed by a sudden decrease in fluorescence intensity. These steps correspond to the photobleaching of individual molecules. We have used a step-detection algorithm that we developed previously (4) to identify steps from these real-time fluorescence traces. Measurement of this 'step' size yields the fluorescence intensity of a single Alexa-594 fluorophore, which can be used as an internal reference to convert the initial fluorescence intensity of individual liposomes to the number of Alexa-594 fluorophores, as we have done previously for individual HIV-1 virions (2) and individual protein-conjugated liposomes (3) using the same quantitation methodology. (**B**) The histogram of the individual photobleaching step sizes for Alexa-594 molecules (N=247), which could be well described by the sum of two Gaussians (red curve), one centered at 630 ± 15 analog-to-digital units (a.u., mean ± standard error) and the other centered at 1249 ± 40 a.u. Under a statistical significance level of 5%, Pearson's Chi-square test (5) selected the double-Gaussian distribution (P-value=0.88) and rejected the single-Gaussian distribution (P-value=0.02) as the model to describe the data. The difference in peak values is close to twofold. As we have observed previously, the secondary peak may result from the photobleaching of two Alexa-594 molecules that occurred almost simultaneously, which could not be resolved by either the finite camera exposure time or the step-finding algorithm (6, 7). The fluorescence intensity of a single Alexa-594 fluorophore can then be used to calculate the total number of Alexa-594 molecules per SVLS based on a ratio comparison (8, 9) with the initial fluorescence intensity of Alexa-594 associated with individual SVLS. The number of RBD molecules per SVLS was then calculated as the total number of Alexa-594 molecules per SVLS normalized by the average number of Alexa-594 molecules per Fab. (**C**) The distributions of epitope density (ED) for pRBD(DNA1)1 (orange), pRBD(DNA1)2 (red), pRBD(DNA1)3 (green), and pRBD(DNA1)4 (blue). These distributions can be well described with Gaussian probability density function, with means and standard deviations of 5 ± 2 for pRBD(DNA1)1 (N=204), 15 ± 4 for pRBD(DNA1)2 (N=182), 31 ± 9 for pRBD(DNA1)3 (N=185), and 43 ± 10 for pRBD(DNA1)4 (N=217), respectively. These values are very close to the value of ED estimated using the ensemble approach as we established previously (Fig. 1F) (3, 10-12).

Fig. S2. Low or undetectable Ag-specific IgM or IgG2c in mice of B6 genetic background upon a single subcutaneous injection of SVLS without iNA.

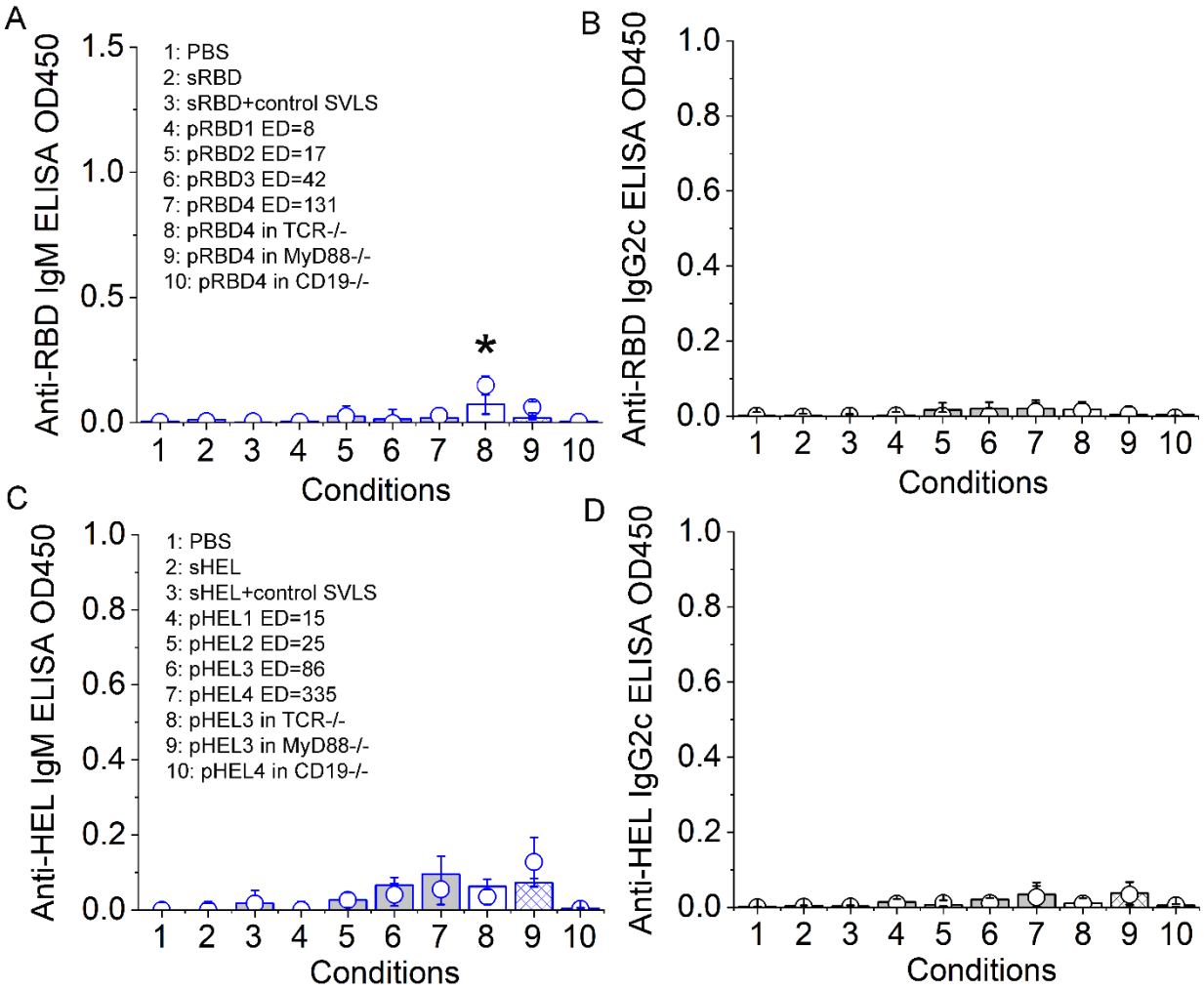

(**A**)(**B**) ELISA OD values for RBD-specific IgM (A) and IgG2c (B) antibody from 1:100 diluted mouse sera after a single subcutaneous injection using various agents listed in the inset with no additional adjuvant. The dose of RBD was 0.24 µg per animal for Conditions 2 through 10. ED refers to epitope density. (**C**)(**D**) ELISA OD values for HEL-specific IgM (C) and IgG2c (D) antibody from 1:100 diluted mouse sera after a single inoculation using various agents listed in the inset. The dose of HEL was 0.3 µg per animal for Conditions 2 through 10. Sera from Day 5 are shown in circles and those from Day 11 post immunization are shown in columns. Graphs depict N=4 mice and are representative of two independent experiments. Throughout Fig. S2, Conditions 1 through 7 were for wtB6 mice. Conditions 8 through 10 were for gene knockout mice of B6 genetic background, with Condition 8 as $TCR^{-/-}$, Condition 9 as $MyD88^{-/-}$ and Condition 10 as $CD19^{-/-}$, following the descriptions in the main text. The pairwise statistical difference between Condition 1 and others on Day 5 was determined by Student's T-test and only Condition 8 in (A) (indicated by the *) shows statistical significance, with p-value < 0.05. Error bars represent the standard errors (N=4).

Fig. S3. Ag-specific IgM and IgG subclasses in BALB/c mice upon a single subcutaneous injection of SVLS without iNA.

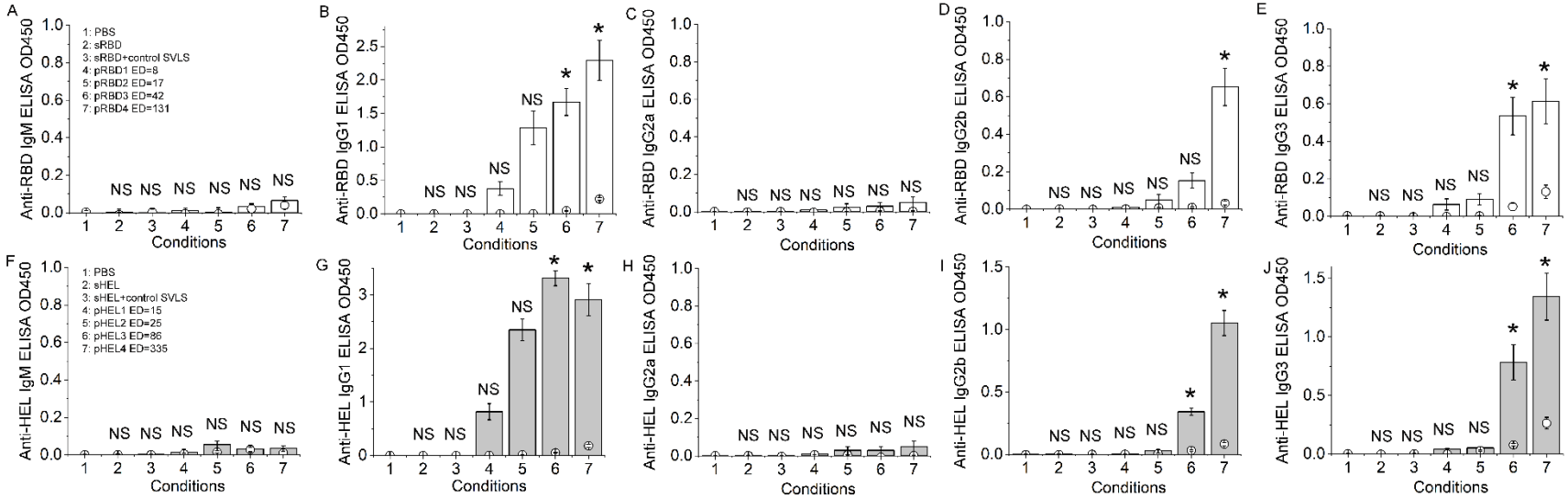

(**A**) through (**E**) ELISA OD values for RBD-specific IgM (A), IgG1 (B), IgG2a (C), IgG2b (D) and IgG3 (E) antibody from 1:100 diluted mouse sera after a single subcutaneous injection using various agents listed in (A) inset with no additional adjuvant. The dose of RBD per injection was 0.24 µg for conditions 2 through 10. (**F**) through (**J**) ELISA OD values for HEL-specific IgM (F), IgG1 (G), IgG2a (H), IgG2b (I) and IgG3 (J) antibody from 1:100 diluted mouse sera after a single subcutaneous injection using various agents listed in (F) inset with no additional adjuvant. The dose of HEL per injection was 0.3 µg for conditions 2 through 10. Throughout, PBS injection (condition 1) was used as a reference to determine the pairwise statistical difference between data points by Student's T-test for all panels. The statistical difference was denoted using the same set of symbols as Fig. 2. Error bars represent the standard errors (N=4).

Fig. S4. Ag-specific IgG subclasses in BALB/c mice upon a single subcutaneous injection of pRBD(DNA1), pHEL(DNA1) or Qβ conjugates.

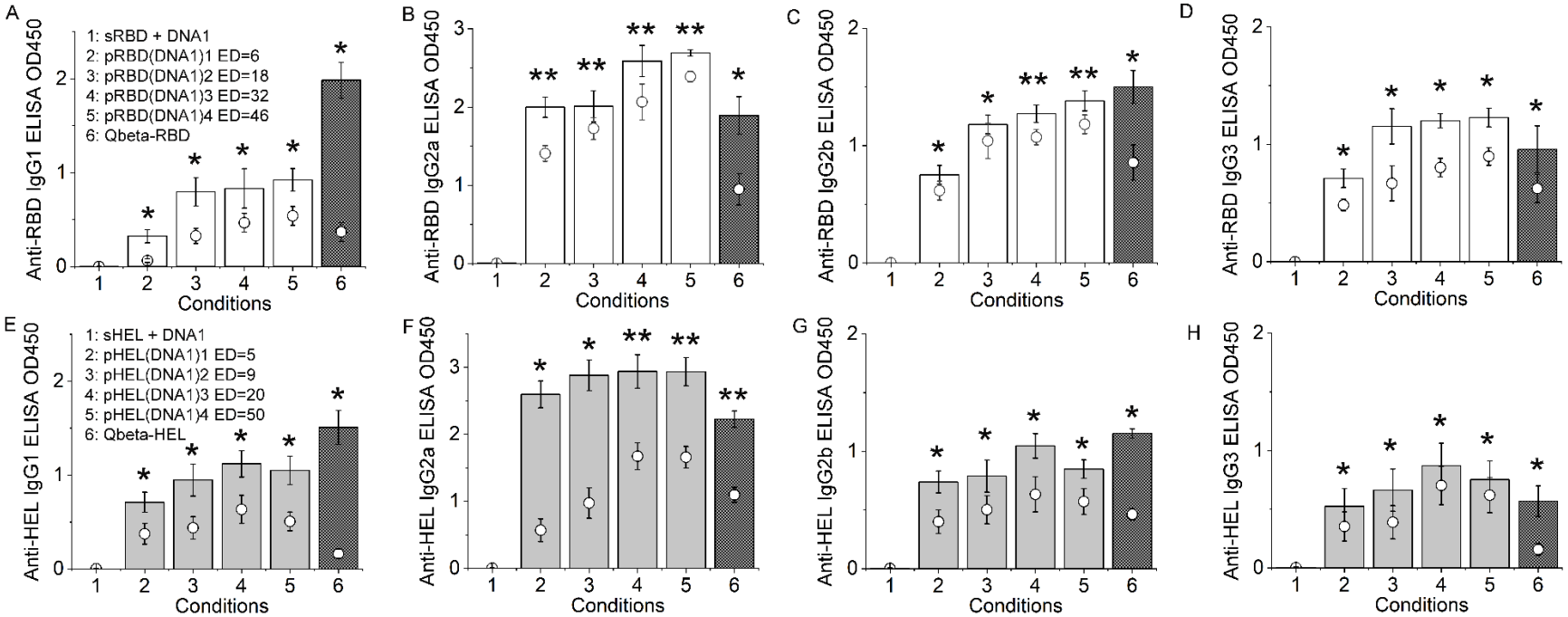

(**A**) through (**D**) ELISA OD values for RBD-specific IgG1 (A), IgG2a (B), IgG2b (C) and IgG3 (D) antibody from 1:100 diluted mouse sera after a single subcutaneous injection using various agents listed in (A) inset with no additional adjuvant. Throughout, the dose of RBD per injection was 0.24 µg for conditions 1 through 6. An admixture of soluble RBD and DNA1 (condition 1) was used as a reference to determine the pairwise statistical difference between data points by Student's T-test. (**E**) through (**H**) ELISA OD values for HEL-specific IgG1 (E), IgG2a (F), IgG2b (G) and IgG3 (H) antibody from 1:100 diluted mouse sera after a single subcutaneous injection using various agents listed in (E) inset with no additional adjuvant. Throughout, the dose of HEL per injection was 0.1 µg for conditions 1 through 6. An admixture of soluble HEL and DNA1 (condition 1) was used as a reference to determine the pairwise statistical difference between data points by Student's T-test. The statistical difference was denoted using the same set of symbols as Fig. 2. Error bars represent the standard errors (N=4). The dose of DNA1 in the admixture with soluble proteins was 1 nmol.

Fig. S5. Ag-specific IgM in mice of B6 genetic background and BALB/c mice upon a single subcutaneous injection of SVLS with iNA or Qβ-conjugates.

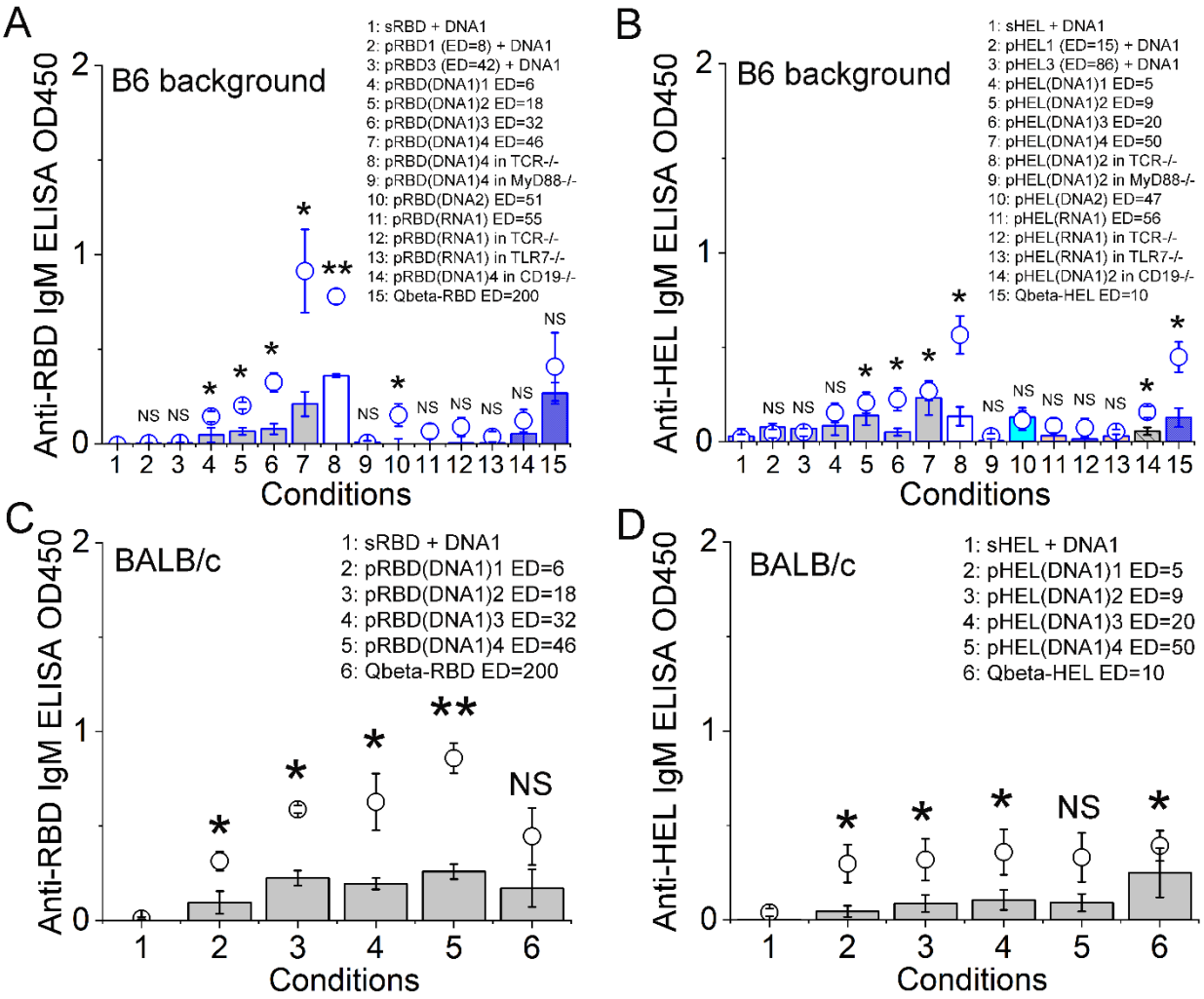

(**A**) ELISA OD values for RBD-specific IgM antibody from 1:100 diluted mouse sera after a single subcutaneous injection using various agents listed in (A) inset with no additional adjuvant in mice of B6 genetic background. The dose of RBD per injection was 0.24 µg for conditions 1 through 15. (**B**) ELISA OD values for HEL-specific IgM antibody from 1:100 diluted mouse sera after a single subcutaneous injection using various agents listed in (B) inset with no additional adjuvant in mice of B6 genetic background. The dose of HEL per injection was 0.1 µg for conditions 1 through 15. (**C**) ELISA OD values for RBD-specific IgM antibody from 1:100 diluted mouse sera after a single subcutaneous injection using various agents listed in (C) inset with no additional adjuvant in BALB/c mice. The dose of RBD per injection was 0.24 µg for conditions 1 through 6. (**D**) ELISA OD values for HEL-specific IgM antibody from 1:100 diluted mouse sera after a single subcutaneous injection using various agents listed in (D) inset with no additional adjuvant in BALB/c mice. The dose of HEL per injection was 0.1 µg for conditions 1 through 6. For each panel above, the respective Condition 1 was used as a reference to determine the pairwise statistical difference between data points within each panel by Student's T-test. Throughout, the statistical difference was denoted using the same set of symbols as Fig. 2. Error bars represent the standard errors (N=4). The dose of DNA1 in admixture with soluble proteins was 1 nmol.

Table S1. List of SVLS used in current study, together with the respective epitope density (ED), and the average number of internal nucleic acid (iNA) molecules per structure.

S1A:

Name of SVLS	ED*	# of iNA per SVLS
pRBD1	8±2	0
pRBD2	17±2	0
pRBD3	42±3	0
pRBD4	131±9	0
pRBD(DNA1)1	6±1	135±3
pRBD(DNA1)2	18±2	140±4
pRBD(DNA1)3	32±2	152±5
pRBD(DNA1)4	46±2	139±3
pRBD(DNA2)	51±3	138±3
pRBD(RNA1)	55±2	147±4

S1B:

Name of SVLS	ED*	# of iNA per SVLS
pHEL1	15±2	0
pHEL2	25±2	0
pHEL3	86±4	0
pHEL4	335±17	0
pHEL(DNA1)1	5±1	118±3
pHEL(DNA1)2	9±2	128±3
pHEL(DNA1)3	20±2	136±4
pHEL(DNA1)4	50±2	130±3
pHEL(DNA2)	47±2	126±4
pHEL(RNA1)	56±3	135±4

(A) RBD-conjugated SVLS and **(B)** HEL-conjugated SVLS. Throughout, the epitope density (ED) refers to the number of antigenic molecules specifically attached to the SVLS surface through maleimide chemistry. The # of iNA per SVLS refers to the average number of nucleic acid molecules encapsulated inside each SVLS. The uncertainties shown for both ED and iNA are standard errors determined from three independent repeats of the same ensemble experiment. Besides the above SVLS used in this study, control SVLS were SVLS that did not have any protein conjugation on surface nor have any iNA encapsulated inside SVLS.

Table S2. Statistical comparison of the titer values between SVLS(DNA1) and respective Ag-Qβ conjugates in wtB6 mice.

S2A:

	pRBD(DNA1)1	pRBD(DNA1)2	pRBD(DNA1)3	pRBD(DNA1)4
Qβ-RBD, D5	0.356	0.537	0.024	1.06e-8
Qβ-RBD, D11	2.88e-8	0.024	0.134	N.A.*

Based on the titer values that we measured for pRBD(DNA1) of varied ED and Qβ-RBD (Fig. 3B), we conducted a one-way ANOVA to test the null hypothesis that the means of titers are equal. The resulting p-values from these tests are reported in Table S2A above. At the 0.05 level, the titer for Qβ-RBD on D5 was not statistically different from that of pRBD(DNA1)1 or pRBD(DNA1)2, and was significantly lower than that of pRBD(DNA1)3 or pRBD(DNA1)4. On D11, the titer for Qβ-RBD was statistically higher than that of pRBD(DNA1)1 or pRBD(DNA1)2, and was not statistically different from that of pRBD(DNA1)3 or pRBD(DNA1)4.

*N.A. the titer values for Qβ-RBD and those from pRBD(DNA1)4 were identical within error.

S2B:

	pHEL(DNA1)1	pHEL(DNA1)2	pHEL(DNA1)3	pHEL(DNA1)4
Qβ-HEL, D5	0.207	0.537	1	1
Qβ-HEL, D11	0.134	0.356	0.356	0.356

Based on the titer values that we measured for pHEL(DNA1) of varied ED and Qβ-HEL (Fig. 3D), we conducted a one-way ANOVA to test the null hypothesis that the means of titers are equal. The resulting p-values from these tests are reported in Table S2B above. At the 0.05 level, the titer for Qβ-HEL on D5 was not statistically different from that of pHEL(DNA1)1, pHEL(DNA1)2, pHEL(DNA1)3 or pHEL(DNA1)4. Similarly, on D11, the titer for Qβ-HEL was not statistically different from that of pHEL(DNA1)1, pHEL(DNA1)2, pHEL(DNA1)3 or pHEL(DNA1)4, either.

Table S3. Statistical comparison of the titer values for SVLS(DNA1) of respective ED between wtB6 and BALB/c mice.

S3A:

	pRBD(DNA1)1	pRBD(DNA1)2	pRBD(DNA1)3	pRBD(DNA1)4
BALB/c, D5	0.356	0.537	0.356	0.134
BALB/c, D11	0.537	0.537	0.134	0.356

Based on the titer values that we measured for pRBD(DNA1) of varied ED in both wtB6 and BALB/c mice (Fig. 3), we conducted a one-way ANOVA to test the null hypothesis that the means of titer values are equal at each respective ED between wtB6 and BALB/c mice. The resulting p-values from these tests are reported in Table S3A above. At the 0.05 level, for each pRBD(DNA1), the titer values from wtB6 mice on D5 or D11 were not statistically different from those in BALB/c mice.

S3B:

	pHEL(DNA1)1	pHEL(DNA1)2	pHEL(DNA1)3	pHEL(DNA1)4
BALB/c, D5	0.537	0.537	0.356	0.356
BALB/c, D11	0.537	0.022	1.408e-8	0.022

Based on the titer values that we measured for pHEL(DNA1) of varied ED in both wtB6 and BALB/c mice (Fig. 3), we conducted a one-way ANOVA to test the null hypothesis that the means of titer values are equal at each respective ED between wtB6 and BALB/c mice. The resulting p-values from these tests are reported in Table S3B above. At the 0.05 level, for each pHEL(DNA1), the titer values from wtB6 mice on D5 were not statistically different from those in BALB/c mice. For pHEL(DNA1)1, the titer values from wtB6 mice on D11 were not statistically different from those in BALB/c mice. However, for pHEL(DNA1)2, pHEL(DNA1)3 and pHEL(DNA1)4, the titer values from BALB/c mice on D11 were statistically higher than those from wtB6 mice.

Table S4. Statistical comparison of the IgG1 ELISA OD450 values for pRBD(DNA1) of respective ED between wtB6 and BALB/c mice.

	pRBD(DNA1)1	pRBD(DNA1)2	pRBD(DNA1)3	pRBD(DNA1)4
BALB/c, D5	0.512	0.075	0.043	0.609
BALB/c, D11	0.085	0.047	0.444	0.940

Based on the IgG1 ELISA OD450 values that we measured for pRBD(DNA1) of varied ED in both wtB6 and BALB/c mice (Fig. 3G and Fig. S5A), we conducted a one-way ANOVA to test the null hypothesis that the means of ELISA OD450 values are equal at each respective ED between wtB6 and BALB/c mice. The resulting p-values from these tests are reported in Table S4 above. At the 0.05 level, the majority of ELISA OD450 values from wtB6 mice on D5 or D11 were not statistically different from those in BALB/c mice.

SI References

1. Y. Pang, H. Song, J. H. Kim, X. Hou, W. Cheng, Optical trapping of individual human immunodeficiency viruses in culture fluid reveals heterogeneity with single-molecule resolution. *Nat Nanotechnol* **9**, 624-630 (2014).
2. M. C. DeSantis, J. H. Kim, H. Song, P. J. Klasse, W. Cheng, Quantitative Correlation between Infectivity and Gp120 Density on HIV-1 Virions Revealed by Optical Trapping Virometry. *J Biol Chem* **291**, 13088-13097 (2016).
3. Z. Chen, J. J. Moon, W. Cheng, Quantitation and Stability of Protein Conjugation on Liposomes for Controlled Density of Surface Epitopes. *Bioconjug Chem* **29**, 1251-1260 (2018).
4. S. G. Arunajadai, W. Cheng, Step detection in single-molecule real time trajectories embedded in correlated noise. *PLoS One* **8**, e59279 (2013).
5. R. D. Evans, Chapter 27. *The Atomic Nucleus (McGraw-Hill)*, Chapter 27 (1969).
6. Y. Pang, H. Song, J. H. Kim, X. Hou, W. Cheng, Optical trapping of individual human immunodeficiency viruses in culture fluid reveals heterogeneity with single-molecule resolution. *Nat Nanotechnol* **9**, 624-630 (2014).
7. X. Hou, W. Cheng, Single-molecule detection using continuous wave excitation of two-photon fluorescence. *Optics letters* **36**, 3185-3187 (2011).
8. V. C. Coffman, J. Q. Wu, Counting protein molecules using quantitative fluorescence microscopy. *Trends Biochem Sci* **37**, 499-506 (2012).
9. J. Lawrimore, K. S. Bloom, E. D. Salmon, Point centromeres contain more than a single centromere-specific Cse4 (CENP-A) nucleosome. *J Cell Biol* **195**, 573-582 (2011).
10. Z. Chen *et al.*, Self-Antigens Displayed on Liposomal Nanoparticles above a Threshold of Epitope Density Elicit Class-Switched Autoreactive Antibodies Independent of T Cell Help. *J Immunol* **204**, 335-347 (2020).
11. W. Y. Wholey *et al.*, Synthetic Liposomal Mimics of Biological Viruses for the Study of Immune Responses to Infection and Vaccination. *Bioconjug Chem* **31**, 685-697 (2020).
12. W. Y. Wholey, S. T. Yoda, W. Cheng, Site-Specific and Stable Conjugation of the SARS-CoV-2 Receptor-Binding Domain to Liposomes in the Absence of Any Other Adjuvants Elicits Potent Neutralizing Antibodies in BALB/c Mice. *Bioconjug Chem* **32**, 2497-2506 (2021).